

Hubbard U and Hund's Exchange J in Transition Metal Oxides: Screening vs. Localization Trends from Constrained Random Phase Approximation

Loïc Vaugier,^{1,2,*} Hong Jiang,^{3,†} and Silke Biermann^{1,2,‡}

¹*Centre de Physique Théorique, Ecole Polytechnique, CNRS UMR 7644, 91128 Palaiseau, France*

²*Japan Science and Technology Agency, CREST, Kawaguchi 332-0012, Japan*

³*Beijing National Laboratory for Molecular Sciences,*

State Key Laboratory of Rare Earth Material Chemistry and Application,

Institute of Theoretical and Computational Chemistry,

College of Chemistry and Molecular Engineering, Peking University, 100871 Beijing, China

(Dated: today)

In this work, we address the question of calculating the local effective Coulomb interaction matrix in materials with strong electronic Coulomb interactions from first principles. To this purpose, we implement the constrained random phase approximation (cRPA) into a density functional code within the linearized augmented plane wave (LAPW) framework.

We apply our approach to the $3d$ and $4d$ early transition metal oxides SrMO_3 ($M=\text{V, Cr, Mn}$) and ($M=\text{Nb, Mo, Tc}$) in their paramagnetic phases. For these systems, we explicitly assess the differences between two physically motivated low-energy Hamiltonians: The first is the three-orbital model comprising the t_{2g} states only, that is often used for early transition metal oxides. The second choice is a model where both, metal d - and oxygen p -states are retained in the construction of Wannier functions, but the Hubbard interactions are applied to the d -states only (“ d -dp Hamiltonian”). Interestingly, since – for a given compound – both U and J depend on the choice of the model, so do their trends within a family of these compounds. In the $3d$ perovskite series SrMO_3 the effective Coulomb interactions in the t_{2g} Hamiltonian decrease along the series, due to the more efficient screening. The inverse – generally expected – trend, increasing interactions with increasing atomic number, is however recovered within the more localized “ d -dp Hamiltonian”. Similar conclusions are established in the layered $4d$ perovskites series Sr_2MO_4 ($M=\text{Mo, Tc, Ru, Rh}$). Compared to their isoelectronic and isostructural $3d$ analogues, the $4d$ 113 perovskite oxides SrMO_3 ($M=\text{Nb, Mo, Tc}$) exhibit weaker screening effects. Interestingly, this leads to an effectively larger U on $4d$ shells than on $3d$ when a t_{2g} model is constructed.

PACS numbers: 71.27.+a, 71.10.Fd, 71.15.Ap, 71.45.Gm

I. INTRODUCTION

Naively, the calculation of the Coulomb repulsion between two charges may seem to be a simple textbook problem. However, calculating this repulsion for two charges in a solid is far from being trivial, as the electronic polarizability screens the Coulomb potential leading to a renormalized repulsion strength. To account for this effect and obtain a quantitative estimation of the interactions, is particularly important in situations where the Coulomb interactions dominate the behavior of the system¹.

The description of the excitations of such strongly correlated materials require a theoretical treatment that goes beyond the one-particle picture of band theory. Simply identifying the Kohn-Sham spectra of density functional theory (DFT) in the local density approximation (LDA)^{2–5} with the many-body spectra, for example, becomes then an inappropriate oversimplification. Popular methods for introducing many-body corrections into this description construct a multi-orbital Hubbard-type Hamiltonian, where explicit interaction terms of Hubbard and Hund form are added. The resulting problem is then e.g. solved within a static mean field theory within the “LDA+U” scheme⁶ or within dynamical mean field theory (DMFT) within the combined “LDA+DMFT”

method^{7–9}. However, the predictive power of such methods crucially relies on a reliable assessment of the interactions. The *ab initio* calculation of these parameters is hence an important issue.

Within the last years, tremendous progress has been made concerning this question, in particular with the advent of the so-called “constrained Random Phase Approximation” (cRPA) as introduced in Ref. [10]. The cRPA provides a systematic first principles technique for the construction of low-energy Hamiltonians where not only the one-particle part of the Hamiltonian but also the interaction part is calculated from first principles, that is without adjustable parameters. The starting point is the choice of an effective low-energy Hilbert space, and the cRPA aims at constructing the *partially screened* interaction that should be used as the *bare* interaction within this space. The procedure should be viewed as the analogue for the interaction term of the familiar “downfolding” techniques used for the one-body part of the Hamiltonian^{11,12}. Matrix elements of the effective partially screened interaction are identified with the Hubbard and Hund’s interaction matrices for the effective low-energy Hamiltonian, and the corresponding parametrizations in terms of Hubbard U and Hund’s rule J can be explicitly constructed.

In this work, we have implemented the constrained

random phase approximation (cRPA)¹⁰ within the full-potential augmented plane wave ((L)APW+lo) framework into the popular density functional code WIEN2K¹³. Our approach allows for the calculation of the Coulomb interaction matrix elements in a localized basis set, and can be combined with many-body techniques working in this framework, such as the recent implementation of LDA+DMFT within the same basis set¹⁴. We illustrate the power of our approach on the $3d$ and $4d$ transition metal oxides SrMO_3 ($M = \text{V, Cr, Mn, Nb, Mo, Tc}$) and Sr_2MO_4 ($M = \text{Mo, Tc, Ru, Rh}$).

It has been argued early on^{15,16} that in systems where the behavior of the correlated orbitals is sufficiently close to a purely atomic description, the Hubbard and Hund interactions acquire the status of physical observables, directly measurable e.g. in spectroscopy experiments. As a consequence of negligible interorbital hybridizations, a natural basis set for the definition of U and J (the atomic one) emerges from the physical situation in these cases. Here, we adopt a more general point of view, defining Hubbard and Hund interactions even for materials where hybridization between states of different orbital character is too strong to allow for uniquely defined atomic orbitals to emerge. Even in this general case, Hubbard and Hund interactions can still be defined as useful auxiliary quantities for many-body calculations, but are no longer direct physical observables. We illustrate this issue on the examples of $3d$ and $4d$ transition metal oxides (ranging from correlated metals to Mott insulators), for which we explicitly construct two different many-body models, demonstrating the dependence of U and J on this choice. We stress that, as a direct consequence of this issue, statements on *values* of U and J for a given material are not meaningful pieces of information unless supplemented by the complete description of the model to which they apply, both concerning the choice of the low-energy subspace and of the correlated orbitals.

The paper is organized as follows: in section II, we discuss the context of our work with respect to previous methods for the determination of Hubbard and Hund interaction parameters. A general description of cRPA and of its implementation within the (L)APW+lo framework is given in section III, supplemented by technical issues in Appendix A and a discussion of a parametrization of the Hubbard interaction matrix in terms of Slater parameters in Appendix B. The results of cRPA calculations on the $3d$ and $4d$ series of ternary transition metal oxides SrMO_3 with ($M=\text{V, Cr, Mn}$) and ($M=\text{Nb, Mo, Tc}$) and on the $4d$ layered perovskites Sr_2MO_4 with ($M=\text{Mo, Tc, Ru, Rh}$) are described respectively in Sections IV and V. In the conclusions in Section VI, we discuss implications and perspectives of the present work.

II. HUBBARD AND HUND INTERACTIONS: FROM SPECTROSCOPY TO FIRST PRINCIPLES CALCULATIONS

A. Hubbard U : fitting parameter or calculated quantity?

Historically, the Coulomb energy cost for placing two electrons on an atomic site within a solid - the Hubbard interaction U - was introduced in the single-orbital Hubbard-Kanamori-Gutzwiller model¹⁷⁻¹⁹. U corresponds to the difference between the electron affinity and the ionization energy when respectively adding and removing an electron on the correlated shell (e.g. the d -shell) of a given atom:

$$U = E(d^{n+1}) + E(d^{n-1}) - 2E(d^n), \quad (1)$$

where $E(d^n)$ is the total energy of a system for which n electrons fill a given d shell on a given atom. When the orbital character of the additional or missing charge is specified also, an interaction *matrix* U can be defined. Depending on the degree to which the correlated d -shell retains its atomic character even in the solid, its elements can be parametrized by a small number of (Slater) parameters.

An important step in the determination of U and J was the pioneering work of Sawatzky and co-workers^{15,16,20-22} who fitted the multiplet structure measured in x-ray photoemission, absorption and Auger spectra with configuration-interaction cluster models involving a set of Slater integrals (F^k)^{23,24}. In a very simplified way, $U = F^0$ can be obtained from the Mott gap whereas the other Slater integrals $F^k, k > 0$ can be deduced from atomic Hartree-Fock-like calculations.

Attempts to calculate U from first principles typically rely on constrained density functional approaches²⁵. Such “constrained LDA” (cLDA) approaches²⁶⁻³⁰ are based on the observation that the energy of a system with increased or reduced particle number is in principle accessible within density functional theory. U^{cLDA} is then defined as the derivative of the total energy while constraining the occupation on a given shell. cLDA-type schemes have been implemented e.g. within the linear muffin-tin orbital (LMTO) framework assuming that the LMTO basis functions used in a multi-orbital Hubbard model give a good representation of the localized degrees of freedom. Later on, implementations of cLDA were worked out within various other electronic structure codes, for example, in the (L)APW+lo framework³¹, or in a basis of maximally localized Wannier functions (MLWF)³². We mention moreover the development of alternative linear response formalisms assessing the screened interaction by explicitly perturbing the system^{33,34}.

In 2004, Aryasetiawan and co-workers¹⁰ proposed a scheme nowadays known under the name of “constrained Random Phase Approximation (cRPA)”. The cRPA is a systematic Wilson-like procedure to downfold a system to a low-energy Hamiltonian.

The cRPA method has been implemented within the LMTO in the atomic sphere approximation (ASA) framework, employing the heads of the LMTOs as local orbitals^{10,35} and within the MLWF framework using the full-potential (FP) LMTO³⁶ and the (L)APW+lo basis³⁷. Materials-wise, the Coulomb interactions in several families of oxypnictides, parent compounds of the new Fe-based superconductors have been investigated within cRPA in the MLWF framework³⁸. *3d*, *4d* and *5d* transition metals have been studied in Refs. [37,39,40]. Interestingly, even the pressure dependence of the Coulomb interactions becomes accessible within cRPA⁴¹. A recent attempt to go beyond the cRPA method uses an LDA+U electronic structure instead of the LDA one as input to the cRPA scheme⁴². This technique has been applied to NiO and elemental Gd.

In recent years, several combined LDA+DMFT studies have appeared, which use the *ab initio* Hubbard and Hund interactions calculated from cRPA. More specifically, the spectral properties of the parent compounds of iron-based superconductors LaOFeAs¹⁴ and FeSe⁴³, and of the layered perovskite Sr₂RuO₄⁴⁴ and the spin-orbit Mott insulator Sr₂IrO₄⁴⁵ have been investigated. Except for the cases of Sr₂IrO₄ and Sr₂RhO₄ these works however evaluated the Coulomb interactions in the MLWF basis set whereas the LDA+DMFT calculations were performed in a different basis set.

B. Hubbard U : physical or auxiliary?

As alluded to above, the definition of U as the difference between electron addition and removal energies, directly accessible in spectroscopy measurements, suggested to consider the local Hubbard interaction as the central physical quantity characterising Coulomb interactions in the solid. A change of paradigm was triggered in 2003, when the proposal of a combined GW and dynamical mean field scheme (“GW+DMFT”)^{46,47} led to a generalisation of the notion of U , degrading it at the same time – at least from a conceptual point of view – to a purely auxiliary quantity. Indeed, in the GW+DMFT scheme, a dynamical interaction function $U_{local}(\omega)$ is introduced and (in principle self-consistently) determined such that the resulting fully screened Coulomb interaction W takes its physical value. This is akin to representing the density – within density functional theory – by an auxiliary (Kohn-Sham-) potential, or the local Green’s function in dynamical mean field schemes by a local impurity bath Weiss function. Formally, this leads to the interpretation of screening as a two-step process: U is interpreted as the *bare* interaction within an effective subsystem with reduced number of degrees of freedom (in the case of GW+DMFT, a dynamical local impurity problem). The latter is such as to generate the physical screened Coulomb interaction W . In the same sense, the cRPA as proposed in Ref. [10], defines U by the require-

ment that the corresponding fully screened interaction

$$W = \frac{U}{1 - P^{sub}U} \quad (2)$$

takes its physical value, and P^{sub} is the polarization of the chosen subsystem. The original cRPA calculates both W and P^{sub} from the random phase approximation, but the general treatment in Ref. [48] for example, makes it clear that this is not an essential ingredient. Other choices for P^{sub} have been explored e.g. in Refs. [49, 50, 51, 52].

C. Constrained Screening Approaches (CSA)

In this paragraph, we give a unified description of the above type of approaches, which we will refer to as “constrained screening approaches” (CSA). They have in common to consider Hubbard interactions U as auxiliary quantities, constructed in such a way that the physical fully screened Coulomb interaction W of the original Coulomb problem in the continuum, possibly within some approximation, coincides with the fully screened Coulomb interaction of a chosen subspace when U is applied as a bare interaction to this subspace. The first step is thus the choice of a subsystem with reduced number of degrees of freedom. In the “GW+DMFT” approach or in the approach of Ref. [52] which directly constructs an impurity problem, this is a local problem. In the constrained random phase approximation (cRPA), as proposed in Ref. [10], this is a low-energy subspace for which a Hubbard model is to be defined. Other choices, as for example subspaces of reduced dimension are also possible; see e.g. Ref. [50] for dimensional downfolding to a 2d-lattice model or Refs. [51,52] for the direct construction of a local model.

The requirement of the physical W be represented by this effective problem (either its local part only, as in GW+DMFT, or with its full momentum-dependence as in the case of the lattice cRPA) leads to a formal relation of U and W involving the polarization P^{sub} of the subsystem: $U^{-1} - W^{-1} = P^{sub}$, that is, U is the partially screened Coulomb interaction, screened by all processes present in the original system except those contained in P^{sub} . For the GW+DMFT scheme, one simply has $P^{sub} = P^{imp}$, the polarization of the dynamical impurity model. In constrained screening approaches geared at the construction of a lattice model (rather than a local one) one sets P^{sub} equal to the polarization P^d of a low-energy correlated subspace. For obvious reasons, in practical calculations equivalent approximations should be made on W and P . The constrained random phase approximation¹⁰, can thus be viewed as a special case, in which both, W and P^{sub} are calculated within the random phase approximation.

In practice, we start by choosing a set of degrees of freedom around the Fermi level in order to generate a

correlated subspace \mathcal{C} of the full Hilbert space. The conceptual division of the Hilbert space into a reference space \mathcal{C} and the remaining degrees of freedom leads to the following decomposition of the response of the system to an external perturbation, expressed by the polarization P :

$$P = P^{sub} + P^r, \quad (3)$$

Here, P^{sub} denotes the polarization within the correlated subspace \mathcal{C} , and, by definition, $P^r = P - P^{sub}$ is a constrained polarization, in which the contributions of the target degrees of freedom have been projected out. The constrained polarization leads to the partial dielectric function ϵ^r

$$\epsilon^r(1, 2) = \delta(1 - 2) - \int d3 P^r(1, 3)v(3, 2). \quad (4)$$

We use here a shorthand notation that consists in representing time (τ) and possible spatial degrees of freedom by a number. In the case of the usual lattice cRPA, for example, this number would thus represent $(\mathbf{r} \tau)$, in the case of local subsystems it would be the time variable. The *partially* screened interaction W^r can then be defined as follows:

$$W^r(1, 2) \equiv \int d3 \epsilon_r^{-1}(1, 3)v(3, 2). \quad (5)$$

A simple algebraic manipulation shows that further screening of W^r by the polarization P^{sub} , or, equivalently, by the low-energy effective dielectric function

$$\epsilon_{sub}(1, 2) = \delta(1 - 2) - \int d3 P^{sub}(1, 3)W^r(3, 2). \quad (6)$$

allows to retrieve the fully screened interaction W :

$$W(1, 2) \equiv \int d3 \epsilon_{sub}^{-1}(1, 3)W^r(3, 2). \quad (7)$$

This property of W^r suggests that it can be identified as the effective bare interaction within the low-energy subspace. More precisely, matrix elements of the static value of W^r in the localized basis set can be interpreted as forming the interaction matrices :

$$U_{....} \equiv \langle .. | W^r | .. \rangle. \quad (8)$$

The following remark is in order here: in fact, the obtained interactions are *frequency-dependent* because of the frequency dependence of the polarization P^r (Eq. 5). This is a physical effect, since the response of the electrons in the solid to an external perturbation depends on the frequency of the latter. In particular, the electrons do not respond to a high-frequency oscillating electric field whose frequency exceeds any electronic energy scale, that is, the electronic polarizability vanishes at high frequency and the partially screened Coulomb interaction W^r coincides, in this limit, with the bare Coulomb interaction. cRPA in principle provides us with the spectrum of

the dynamical interaction whose combination with many-body solvers such as extended dynamical mean field theory is currently receiving much attention^{53–55}. In particular, it was shown how inclusion of the high-energy tail of the energy-dependent Coulomb interaction leads, in the spectral functions, to pronounced shifts of weight to higher energies and a concomitant additional renormalization at low energies^{53,54}. Recently, an explicit expression for these renormalisations was derived⁵⁵, yielding a prescription for the construction of a low-energy Hubbard-like model with static Hubbard and Hund interactions where the high-energy screening effects are already incorporated. Specifically, it was argued that the static interaction matrices to be used in such a construction are precisely the ones obtained from constrained screening approaches in the static limit ($\omega \rightarrow 0$). These are the subject of the present work.

III. THE CONSTRAINED RANDOM PHASE APPROXIMATION

A. Constrained Polarization

While the conceptual construction of the Hubbard interactions is general and in principle independent of the specific choice of the subsystem, the construction acquires its sense from a Wilson-like argument, when the reference system is a low-energy subspace: $P^{sub} = P^d$, where the subscript d refers to a low-energy correlated target space. The constrained random phase approximation then corresponds to the choice of calculating both, the polarization of this subspace and the total polarization within the RPA approximation. If we assume that the low-energy bands that span the correlated subspace do not energetically overlap with the remaining bands, the \mathcal{C} -restricted polarization reads as

$$P^d(\mathbf{r}, \mathbf{r}'; \omega) = \sum_{\mathbf{k}, d}^{\text{occ}} \sum_{\mathbf{k}', d'}^{\text{unocc}} \psi_{d\mathbf{k}}^*(\mathbf{r}) \psi_{d'\mathbf{k}'}(\mathbf{r}) \psi_{d'\mathbf{k}'}^*(\mathbf{r}') \psi_{d\mathbf{k}}(\mathbf{r}') \times \left\{ \frac{1}{\omega - \epsilon_{d'\mathbf{k}'} + \epsilon_{d\mathbf{k}} + i\eta} - \frac{1}{\omega + \epsilon_{d'\mathbf{k}'} - \epsilon_{d\mathbf{k}} - i\eta} \right\} \quad (9)$$

where $\epsilon_{d\mathbf{k}}$ are the energies of the Bloch states, $\psi_{d\mathbf{k}}(\mathbf{r})$, that span \mathcal{C} . The polarization P^r is then deduced from Eq. (3).

B. Definition of the correlated subspace

The choice of the “target” degrees of freedom – or low-energy subspace – is obviously not unique. Two different “downfolded” Hamiltonians will not lead to the same effective interactions. However, both choices should yield the same results for physical observables at the end, under the condition that both models are appropriate for catching the relevant physics of the system.

In the following, we assume that the band structure – as in the perovskite materials considered in this paper – is such that the orbital character of the “correlated species” (here the $3d$ or $4d$ orbitals) is dominantly spread over a subset of bands that are not entangled with bands of other orbital characters. In other words, the Hilbert space can be split into a correlated and an itinerant subspace that – for every \mathbf{k} -point in the first Brillouin zone – are separated in energy. The situation of entangled subspaces require specific treatments that will be reported elsewhere (see also Refs. [37,40]).

Our implementation is based on the full-potential (L)APW+lo code WIEN2K¹³, and the construction of localized orbitals according to the procedure implemented in Ref. [14]. In the case of separated bands in the sense described above, this construction results in a set of Wannier functions $\{|\phi_{\mathbf{k}m}^{\alpha\sigma}\rangle\}$ that span the “target” space \mathcal{C} . The index m denotes an orbital quantum number, α is an atomic index inside a given unit cell centered at \mathbf{R} and σ is the spin degree of freedom.

The practical construction of the $\{|\phi_{\mathbf{k}m}^{\alpha\sigma}\rangle\}$ proceeds as follows: one starts by choosing the dominant orbital character of the states that are to be considered as correlated, as well as an energy window \mathbb{W} that contains at least all bands whose majority character is the correlated one. One then uses a set of localized atomic orbitals of the chosen character $\{|\chi_{\mathbf{k}m}^{\alpha\sigma}\rangle\}$ and calculates their projection onto the Bloch states that lie in the energy window \mathbb{W} :

$$|\tilde{\chi}_{\mathbf{k}m}^{\alpha\sigma}\rangle = \sum_{\nu \in \mathbb{W}} \langle \psi_{\mathbf{k}\nu}^{\sigma} | \chi_{\mathbf{k}m}^{\alpha\sigma} \rangle | \psi_{\mathbf{k}\nu}^{\sigma} \rangle. \quad (10)$$

The set of wave functions $\{|\tilde{\chi}_{\mathbf{k}m}^{\alpha\sigma}\rangle\}$ is then subject to an orthonormalization procedure, yielding the orthonormal Wannier basis $\{|\phi_{\mathbf{k}m}^{\alpha\sigma}\rangle\}$. It is an easy task to verify that this set is indeed complete within the selected subspace.

In order to be able to transform back and forth between the Kohn-Sham and the Wannier basis, a set of “Wannier” projectors $P_{m\nu}^{\alpha\sigma}(\mathbf{k})$ are defined as follows :

$$P_{m,\nu}^{\alpha\sigma}(\mathbf{k}) \equiv \langle \phi_{\mathbf{k}m}^{\alpha\sigma} | \psi_{\mathbf{k}\nu}^{\sigma} \rangle, \quad (11)$$

and with simplified notations, $L = (m, \alpha, \sigma)$,

$$|\phi_{\mathbf{k}L}\rangle = \sum_{\nu \in \mathbb{W}} P_{L\nu}^*(\mathbf{k}) | \psi_{\mathbf{k}\nu}^{\sigma} \rangle. \quad (12)$$

The atom-centered Wannier functions in which the Hubbard model is formulated are finally obtained from a simple Fourier transformation from the reciprocal to the direct space:

$$|\phi_{\mathbf{R}L}\rangle = \frac{1}{\sqrt{\mathcal{N}}} \sum_{\mathbf{k}} e^{-i\mathbf{k} \cdot \mathbf{R}} |\phi_{\mathbf{k}L}\rangle, \quad (13)$$

where \mathcal{N} corresponds to the number of \mathbf{k} vectors inside the first Brillouin zone.

As mentioned before, in general the choice of the different subspaces is not unique. Depending on the material

and the physical quantities considered, one has to decide for example whether to include ligand states in the model or not. For the oxide compounds considered in this work, two natural choices appear. We use the notations previously introduced in Ref. [56].

“ t_{2g} - t_{2g} Hamiltonian”: Due to the octahedral crystal field of the oxygen ligands, the d states of the metal ion M^{4+} in SrMO_3 are split into t_{2g} and e_g bands. The t_{2g} bands are partially filled (with one electron in SrVO_3 three electrons in SrMnO_3) whereas the e_g states are empty. In a quite intuitive way, one can choose the t_{2g} bands as the low-energy degrees of freedom in the cRPA downfolding procedure. The correlated subspace $\mathcal{C}_{t_{2g}}$ thus includes only the t_{2g} degrees of freedom. To construct this subspace explicitly, a set of Wannier functions with the t_{2g} character is constructed out of Kohn-Sham bands within the energy window $\mathbb{W}_{t_{2g}}$. The energy window $\mathbb{W}_{t_{2g}}$ is chosen such as only t_{2g} bands are included. To calculate the constrained polarization P^r , transitions from and to the target t_{2g} bands included in $\mathbb{W}_{t_{2g}}$ are removed from the total polarization (Eq. 3). A method based on the Kohn-Sham indices or on an energy window can be employed to label the transitions that have to be eliminated, since the t_{2g} bands do not energetically overlap with p and e_g ones.

We finally obtain the interaction parameters that correspond to a $\mathcal{C}_{t_{2g}}$ -restricted lattice Hamiltonian. We call this model the “ t_{2g} - t_{2g} Hamiltonian”, where the first index refers to the majority character of the bands that are cut out from the screening process when going from P to P^r , and the second refers to the majority character of the bands that are used to construct the Wannier functions in which matrix elements are taken.

“ d - dp Hamiltonian”: Alternatively, one can choose as correlated subspace \mathcal{C}_{dp} the space that contains also the e_g degrees of freedom in addition to the t_{2g} ones. In an octahedral crystal field, however, the $(d_{3z^2-r^2}, d_{x^2-y^2})$ orbitals strongly hybridize with the ligands, forming bonding and anti-bonding bands. The former are dominantly of ligand- p character, with substantial weight of the transition metal d contribution, however, while the latter are dominantly formed by the e_g states, with admixture from ligand p states. This situation suggests to use for the construction of the Wannier functions an extended dp energy window \mathbb{W}_{dp} that includes the whole d manifold as well as the p one. It could thus appear natural in this context to construct a low-energy effective Hamiltonian, where both, d - and p -states, are treated as correlated states. Treating Coulomb interactions between the in general rather extended p electrons as local, however, seems to be a more drastic approximation than treating these interactions in a static mean field fashion. In practice, it is thus more common to describe oxides within a hybrid model, where the Wannier functions are constructed within an extended dp window, while applying Hubbard interaction terms only to the d -manifold. Analogous constructions have for example been performed for iron pnictide compounds⁵⁶ where the

Fe- d states were considered as correlated while “uncorrelated” pnictogen or oxygen states had been included for the sake of the construction of sufficiently localized Wannier functions. The philosophy that is currently taken in this context is then to construct the constrained polarization P^r from the total polarization by cutting off the transitions from and to the target d bands. The low-energy subspace described by the Hamiltonian is however composed of the full d - and p -manifolds. Following the notation of reference⁵⁶ we call this hybrid model the “ d - dp Hamiltonian”.

C. Calculated quantities

1. Definition of matrix elements

The cRPA method allows to calculate the effective interaction matrix elements of a low-energy lattice Hamiltonian expanded in the localized basis set, $\{|\phi_{\mathbf{R}L}\rangle\}$:

$$U_{L_1 L_2 L_3 L_4}^{\mathbf{R}_1 \mathbf{R}_2 \mathbf{R}_3 \mathbf{R}_4}(\omega) \equiv \langle \phi_{\mathbf{R}_1 L_1} \phi_{\mathbf{R}_2 L_2} | W^r(\omega) | \phi_{\mathbf{R}_3 L_3} \phi_{\mathbf{R}_4 L_4} \rangle \quad (14)$$

$$= \iint d\mathbf{r} d\mathbf{r}' \phi_{\mathbf{R}_1 L_1}^*(\mathbf{r}) \phi_{\mathbf{R}_2 L_2}(\mathbf{r}) W^r(\mathbf{r}, \mathbf{r}'; \omega) \times \phi_{\mathbf{R}_3 L_3}^*(\mathbf{r}') \phi_{\mathbf{R}_4 L_4}(\mathbf{r}'). \quad (15)$$

By expanding the localized orbitals into the Kohn-Sham states within the energy window \mathbb{W} , the interaction matrix elements read (Appendix A) :

$$U_{L_1 L_2 L_3 L_4}^{\mathbf{R}_1 \mathbf{R}_2 \mathbf{R}_3 \mathbf{R}_4}(\omega) = \mathcal{N}^{-2} \sum_{\mathbf{k}_1 \mathbf{k}_2 \mathbf{k}_3 \mathbf{k}_4} e^{i(\mathbf{k}_1 \mathbf{R}_1 - \mathbf{k}_3 \mathbf{R}_3 + \mathbf{k}_2 \mathbf{R}_2 - \mathbf{k}_4 \mathbf{R}_4)} \times \sum_{\nu_1 \nu_2 \nu_3 \nu_4 \in \mathbb{W}} P_{L_1 \nu_1}(\mathbf{k}_1) [P_{L_3 \nu_3}(\mathbf{k}_3)]^* \times \langle \psi_{\mathbf{k}_1 \nu_1} \psi_{\mathbf{k}_2 \nu_2} | W^r(\omega) | \psi_{\mathbf{k}_3 \nu_3} \psi_{\mathbf{k}_4 \nu_4} \rangle [P_{L_4 \nu_4}(\mathbf{k}_4)]^* P_{L_2 \nu_2}(\mathbf{k}_2). \quad (16)$$

Analogously, one can compute the fully screened interaction,

$$W_{L_1 L_2 L_3 L_4}^{\mathbf{R}_1 \mathbf{R}_2 \mathbf{R}_3 \mathbf{R}_4}(\omega) \equiv \langle \phi_{\mathbf{R}_1 L_1} \phi_{\mathbf{R}_2 L_2} | W(\omega) | \phi_{\mathbf{R}_3 L_3} \phi_{\mathbf{R}_4 L_4} \rangle, \quad (17)$$

and the bare interaction,

$$v_{L_1 L_2 L_3 L_4}^{\mathbf{R}_1 \mathbf{R}_2 \mathbf{R}_3 \mathbf{R}_4} \equiv \langle \phi_{\mathbf{R}_1 L_1} \phi_{\mathbf{R}_2 L_2} | v | \phi_{\mathbf{R}_3 L_3} \phi_{\mathbf{R}_4 L_4} \rangle. \quad (18)$$

While the procedure is in principle directly applicable also to non-local interactions, we will restrict the discussion in the following to local (that is intra-atomic) interactions ($\mathbf{R}_1 = \mathbf{R}_2 = \mathbf{R}_3 = \mathbf{R}_4$). The interaction matrix elements are denoted $U_{m_1 m_2 m_3 m_4}^{\mathcal{S}}$ where m refers to angular quantum numbers indicating the dominant orbital character of the local basis set and \mathcal{S} to the symmetry of the crystal field used for constructing the localized basis $\{|\phi_{\mathbf{R}L}\rangle\}$ (in our case, cubic harmonics or spherical harmonics). The four-index interaction matrix within the

cubic harmonics, $U_{m_1 m_2 m_3 m_4}^{\text{cubic}}$, includes in principle not only density-density interaction terms. Reduced interaction matrices, $U^{\sigma\bar{\sigma}}, U^{\sigma\sigma}$, for the density-density interaction with cubic symmetry between opposite spin and parallel spin electrons respectively, can be defined as follows :

$$U_{mm'}^{\sigma\bar{\sigma}} \equiv U_{mm'mm'}^{\text{cubic}} = \langle \phi_m \phi_{m'} | W^r(0) | \phi_m \phi_{m'} \rangle \quad (19)$$

$$J_{mm'} \equiv U_{mm'mm'}^{\text{cubic}} = \langle \phi_m \phi_{m'} | W^r(0) | \phi_{m'} \phi_m \rangle \quad (20)$$

$$U_{mm'}^{\sigma\sigma} \equiv U_{mm'mm'}^{\text{cubic}} - J_{mm'}. \quad (21)$$

For practical reasons, and in order to simplify its further use within many-body techniques, it is convenient to parametrize these matrices by a reasonable number of parameters. Common practice and physical insight suggests the popular choice of the Slater parametrization. Based on the assumption of spherical symmetry, this form is strictly valid only for atoms, but yields – for sufficiently localized atomic-like states – a good approximation for the correlated shells of a solid.

2. Slater integrals

The parametrization by Slater integrals^{23,24,57} makes use of the specific form of the angular momentum integrals in the atomic case, reducing the problem to the calculation of a restricted number of radial integrals (3 in the case of a d shell, 4 in the case of a f shell). Useful relations are summarized in Appendix B. The Slater integrals $F^k(\omega)$ can be employed for building the symmetrized interaction matrix $\bar{U}_{m_1 m_2 m_3 m_4}^{\text{cubic}}(\omega)$ with cubic symmetry as follows:

$$\bar{U}_{m_1 m_2 m_3 m_4}^{\text{cubic}}(\omega) = \sum_{m'_1 m'_2 m'_3 m'_4} \mathcal{S}_{m_1 m'_1} \mathcal{S}_{m_2 m'_2} \times \left\{ \sum_{k=0}^{2l} \alpha_k(m'_1, m'_2, m'_3, m'_4) F^k(\omega) \right\} \mathcal{S}_{m'_3 m_3}^{-1} \mathcal{S}_{m'_4 m_4}^{-1}, \quad (22)$$

where α_k are the Racah-Wigner numbers (Appendix B) and \mathcal{S} is the transformation matrix from spherical harmonics to cubic ones.

Different conventions exist for the Hubbard U parameter. We follow the convention of identifying U with the Slater integral F^0 (Refs. [6,58]) related to matrix elements of the interaction as a simple average over all possible pairs of orbitals:

$$U \equiv \frac{1}{(2l+1)^2} \sum_{mm'} \sum_{k=0}^{2l} \alpha_k(m, m', m, m') F^k \quad (23)$$

$$= F^0. \quad (24)$$

Hund’s exchange J is given by⁵⁸ :

$$J \equiv \frac{1}{2l(2l+1)} \sum_{m \neq m'} \sum_k \alpha_k(m, m', m', m) F^k. \quad (25)$$

Using Slater integrals manipulations, it can be shown that :

$$J = \begin{cases} (F^2 + F^4)/14 & (\text{for } d \text{ shells}) \\ (286F^2 + 195F^4 + 250F^6)/6435 & (\text{for } f \text{ shells}), \end{cases} \quad (26)$$

Analogously, one can define bare parameters, v and J_{bare} , and fully screened ones, W and J_{screened} , using the appropriate Slater integrals. The underlying assumption of this construction is that all three, bare, partially screened and fully screened interactions are spherically symmetric, that is keep the form imposed by the purely atomic angular momentum integrals. In general, this can be expected to be a good approximation for the bare interaction if the orbitals are sufficiently localized and thus atomic-like. In how far it is a good description for the partially and fully screened interaction depends on in how far screening acts as to break the spherical symmetry, inducing additional anisotropies through hybridizations in the local environment in the solid.

Based on Eq. 22, one can extract Slater-symmetrized effective interactions for the whole d shell, corresponding to density-density interactions within the t_{2g} subspace, the e_g subspace and also between the t_{2g} and e_g ²⁴. For further comparison with the interactions between t_{2g} orbitals but within the t_{2g} - t_{2g} model, we will restrict ourselves to the Slater-symmetrized interactions for the t_{2g} subspace only :

$$\bar{U}_{mm} = F^0 + \frac{4}{49}F^2 + \frac{4}{49}F^4 \quad (27)$$

$$\bar{U}_{mm'} = F^0 - \frac{2}{49}F^2 - \frac{4}{441}F^4 \quad (28)$$

$$\bar{J}_m \equiv \frac{1}{2}(\bar{U}_{mm} - \bar{U}_{mm'}) = \frac{3}{49}F^2 + \frac{20}{441}F^4. \quad (29)$$

3. Hubbard-Kanamori parameters

In the case of large crystal field splittings, the assumption of spherical symmetry of the correlated states is no longer valid, and the appropriate parameters for constructing the t_{2g} -restricted lattice Hamiltonian (t_{2g} - t_{2g}) are the Hubbard-Kanamori parameters²⁴. They are directly calculated from the interaction matrix elements in the $\mathcal{C}_{t_{2g}}$ subspace as follows :

$$\mathcal{U} = \frac{1}{N} \sum_{m=1}^{N=3} U_{mmmm}^{\text{cubic}} \quad (30)$$

$$\mathcal{J} = \frac{1}{N(N-1)} \sum_{m \neq m'}^{N=3} U_{mm'm'm}^{\text{cubic}} \quad (31)$$

$$\mathcal{U}' = \frac{1}{N(N-1)} \sum_{m \neq m'}^{N=3} U_{mm'mm'}^{\text{cubic}}, \quad (32)$$

Analogously, one can define bare parameters, ($\mathcal{V}, \mathcal{J}_{\text{bare}}$), and fully screened ones, ($\mathcal{W}, \mathcal{J}_{\text{screened}}$), by considering

the bare and fully screened interaction matrices, v^{cubic} and W^{cubic} , respectively.

4. Calculated quantities: summary of notations

The Hubbard interaction matrix elements with cubic symmetry are denoted $U_{m_1 m_2 m_3 m_4}^{\text{cubic}}$ (Eq. 16), and the corresponding reduced interaction matrices, $U_{mm'}^{\sigma\bar{\sigma}}, U_{mm'}^{\sigma\sigma}$ (Eqs. 19 and 21).

Within the d - dp Hamiltonian, the average interaction matrix elements between t_{2g} orbitals that are directly calculated with cubic symmetry are denoted $U_{mm}, U_{mm'}$ and J_m for the on-site intra- t_{2g} , inter- t_{2g} and exchange interaction, respectively. Analogous quantities, but for the *bare* situation, $v_{mm}, J_m^{\text{bare}}$, and for the *fully screened* situation, $W_{mm}, J_m^{\text{screened}}$, can be introduced.

We deduce from the Slater integrals parametrization, the Hubbard parameter $U \equiv F^0$ (Eq. 24) and Hund's exchange $J \equiv (F^2 + F^4)/14$ for the d shell (Eq. 26). They are the parameters that should be considered for constructing the interaction Hamiltonian downfolded into the d - dp low-energy subspace chosen (Eq. 22). Analogous parameters but within *bare* (unscreened) repulsions, v and J_{bare} , or within *fully screened* repulsions, W and J_{screened} , are introduced.

Employing Eqs. 27, 28 and 29, Slater-average on-site, \bar{U}_{mm} , and exchange, \bar{J}_m , interactions between t_{2g} orbitals within the d - dp Hamiltonian, can be extracted – and analogously for the *bare*, $\bar{v}_{mm}, \bar{J}_m^{\text{bare}}$ and the *fully screened* $\bar{W}_{mm}, \bar{J}_m^{\text{screened}}$ cases. They correspond to a part only – the t_{2g} one – of the d - dp low-energy Hamiltonian and therefore, should not be taken for parametrizing this Hamiltonian.

Within the t_{2g} - t_{2g} Hamiltonian, the Hubbard-Kanamori terms, $\mathcal{U}, \mathcal{U}', \mathcal{J}$ (Eqs. 30, 31 and 32), refer to the interactions between t_{2g} orbitals within the t_{2g} -restricted Hamiltonian. \mathcal{U} corresponds to the intra-orbital Coulomb repulsion, whereas $\mathcal{U}' (= \mathcal{U} - 2\mathcal{J}$ with cubic symmetry) is the inter-orbital interaction which is reduced by Hund's exchange, \mathcal{J} . They are the appropriate parameters for mapping the low-energy Hamiltonian downfolded into the t_{2g} subspace. Analogous parameters but within *bare* repulsions, $\mathcal{V}, \mathcal{J}_{\text{bare}}$, or within *fully screened* repulsions, $\mathcal{W}, \mathcal{J}_{\text{screened}}$, are also introduced.

IV. HUBBARD INTERACTIONS IN PEROVSKITE TRANSITION-METAL OXIDES SrMO_3 ($M = \text{V, Cr, Mn, Nb, Mo, Tc}$)

A. General trends

We first consider the ternary transition metal oxides SrMO_3 ($M = \text{V, Cr, Mn, Nb, Mo, and Tc}$) in an undistorted cubic perovskite structure. This is the stable structure for SrVO_3 , while for the other compounds this is an idealisation. In this structure, the transition metal

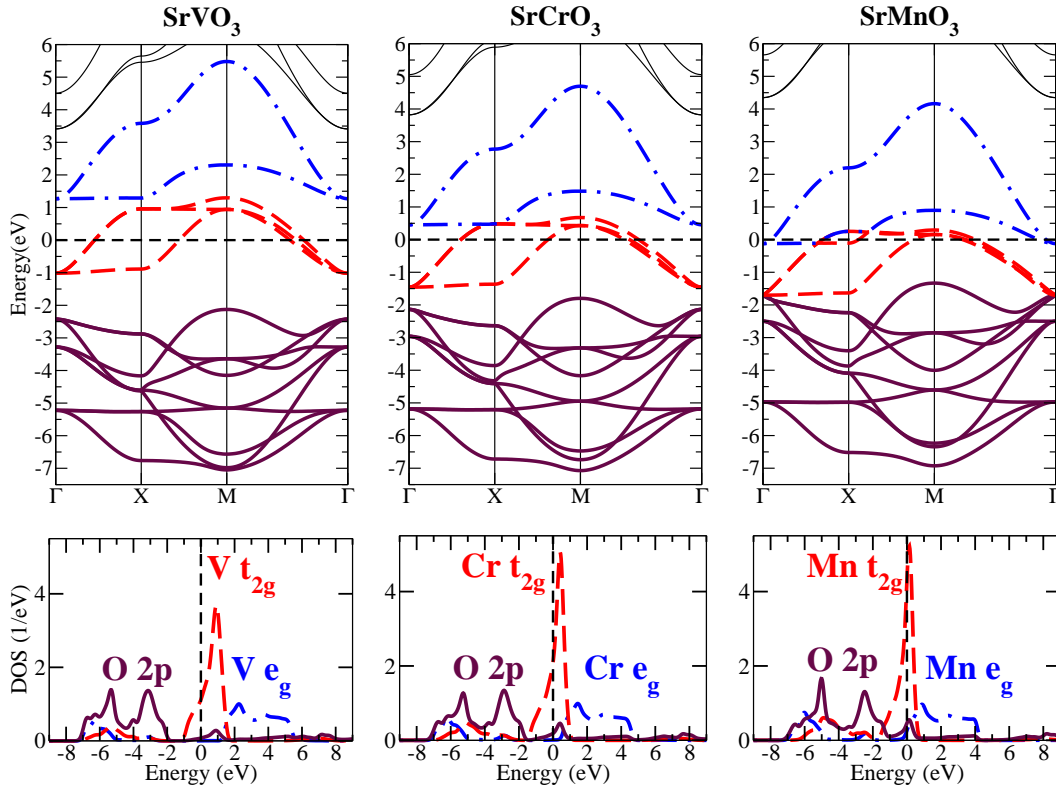


Figure 1: (color online) Electronic band structures (top) and projected density of states (bottom) of SrMO_3 ($M = \text{V, Cr, Mn}$ from left to right) obtained from LDA in the paramagnetic phase. The t_{2g} states are highlighted in red (dash), the e_g 's in blue (dash-dot) and the oxygen p 's in maroon (solid).

Table I: Lattice parameters used for cubic perovskites SrMO_3 and energy windows \mathbb{W} (in eV) for the d - dp and the t_{2g} - t_{2g} models. d and t_{2g} Wannier-like functions are constructed out of the Kohn-Sham states included in \mathbb{W} . Because of the entanglement of the e_g states with Sr-like d states, the d - dp model is not considered for $4d$ SrMO_3 .

	a (Å)	\mathbb{W}_{dp}	$\mathbb{W}_{t_{2g}}$
SrVO_3	3.842	$[-7.5, 5.5]$	$[-1.8, 1.8]$
SrCrO_3	3.820	$[-7.5, 4.7]$	$[-1.7, 1.0]$
SrMnO_3	3.805	$[-7.5, 4.2]$	$[-1.7, 1.0]$
SrNbO_3	3.997		$[-3.0, 2.8]$
SrMoO_3	3.976		$[-3.0, 2.0]$
SrTcO_3	3.950		$[-2.6, 1.3]$

ion is octahedrally coordinated with oxygen ligands, inducing a splitting of the d orbitals of the transition metal into t_{2g} and e_g , where the e_g form bonding and anti-bonding states with the oxygen p . The t_{2g} states form a relatively narrow partially filled band, separated in energy both from the e_g and the p states. There are two important factors that characterise trends in the electronic structure of transition metal (TM) perovskites: 1) the lo-

calization of TM- d orbitals, which increases as the atomic number increases within the same period of the periodic table, and decreases as the atomic number increases in the same group, and 2) the hybridization between transition metal d and O- $2p$ states, which depends on the localization of the d orbitals as well as on the energetic splitting between d and O- $2p$, the charge transfer energy and ligand field Δ_{pd} . The interplay of these two factors, together with the filling of the d manifold, gives rise to extremely intriguing physics and chemistry. The DFT-LDA band structures of the $3d$ and $4d$ transition metal perovskites in their paramagnetic phases are shown in Figs. 1 and 2, respectively. The lattice parameters used in the calculations are listed in Table I.

Due to the contraction of the d orbitals with increasing atomic number, the hybridization between d and p orbitals lessens from the early to the late oxides. Similarly, the charge transfer energy between d and p bands, Δ_{pd} , also decreases, in qualitative agreement with optics experiments^{59,60}. On the other hand, the charge transfer energy is larger in $4d$ than in $3d$, due to the larger orbital extension of the former (Fig. 2).

The narrowing of the $3d$ bands around the Fermi level makes the corresponding oxides prototypical for the interplay between electronic itineracy and localization^{1,61}. The $3d$ -based materials are usually considered as more

“correlated” than their $4d$ analogues due to the more localized character of the $3d$ orbitals. Within the Zaanen-Sawatzky-Allen classification⁶² and the evolution of Δ_{pd} through the series, the early transition metal oxides are more prone to Mott localization whereas charge transfer physics is dominant in the late ones. As commonly found in the literature – although never calculated yet – the local intra-orbital interactions are believed to increase with the atomic number in a similar way as in atomic systems. We show below that the trend for these interactions can differ from the one for atoms and we rationalize this discrepancy within the antagonism between the effects of the orbital localization and the screening.

B. $3d$ perovskites: experimental facts

We now give a brief – and by no means exhaustive – summary of experimental results on the oxide perovskite families, SrMO_3 ($M = \text{V, Cr, Mn}$).

SrVO₃: Among the chosen oxides, SrVO_3 has been intensively investigated both experimentally and theoretically as a prototypical TM oxide that falls in the intermediately correlated regime. Experimentally it is found to be an undistorted paramagnetic metal which has been well characterized by experiments like optics, thermodynamical measurements, transport or angle-integrated and angle-resolved photoemission spectroscopy.^{1,63–67} Photoemission spectra [65,66] show a lower Hubbard band at about 1.7 eV binding energy and a quasiparticle peak characterized by the renormalization factor $Z \approx 0.6$. An electron addition peak $d^1 \rightarrow d^2$ has been identified by inverse photoemission at about 2.5 – 3 eV.⁶⁷ DFT-LDA can give a qualitatively correct description of the band structure of SrVO_3 , as shown in Fig. 1, but a quantitative description including the band renormalisation requires a more accurate treatment of the correlation effects in the d -manifold^{14,50,63,68}.

SrCrO₃: Because of difficulties in the synthesis of SrCrO_3 , only few studies have been conducted. Early work on single crystals with cubic structure⁶⁹ shows a metallic behavior with a Pauli paramagnetic susceptibility. This is in disagreement with a more recent study on polycrystals reporting transport, thermal conductivity and magnetic susceptibility in favor of a non-magnetic insulating state⁷⁰. SrCrO_3 crystals have been also recently reinvestigated within x-ray diffraction studies⁷¹. The common belief found in the literature – supported by density functional calculations – is that a structural transition from a non-magnetic orbitally-degenerate cubic to a distorted tetragonal- maybe antiferromagnetic-structure with orbital ordering could appear below 70 K^{71–73}.

SrMnO₃: At room temperature, SrMnO_3 is found in an hexagonal phase^{74–77} but a cubic phase can be quenched and stabilized in a metastable state down to low temperatures. Both phases are deeply insulating. A G-type antiferromagnetic ordering with a magnetic mo-

Table II: (top) Slater integrals for the d - dp model of SrMO_3 ($M = \text{V, Cr, Mn}$) corresponding to screened (W^r) and bare (v) Coulomb interaction. (bottom) Slater-symmetrized effective interactions between t_{2g} orbitals.

(eV)	F^0	F^4/F^2	J	F_{bare}^0	$F^4/F^2 _{\text{bare}}$	J_{bare}
SrVO_3	3.2	0.795	0.85	19.5	0.652	1.06
SrCrO_3	2.9	0.781	0.85	20.1	0.628	1.06
SrMnO_3	2.8	0.774	0.89	21.2	0.625	1.11
	\bar{U}_{mm}	$\bar{U}_{mm'}$	\bar{J}_m	\bar{v}_{mm}	$\bar{v}_{mm'}$	\bar{J}_m^{bare}
SrVO_3	4.1	2.8	0.65	20.7	19.1	0.81
SrCrO_3	3.9	2.6	0.65	21.4	19.7	0.82
SrMnO_3	3.8	2.4	0.68	22.5	20.8	0.86

ment around $2.6 \mu_B$ emerges below the Néel temperature $T_N \sim 260\text{K}$ ⁷⁵. According to x-ray photoemission and absorption^{78–80}, the spectroscopic properties of SrMnO_3 are rather involved. Indeed, the O- p states are strongly entangled with the lower Hubbard band of t_{2g} character, and the conduction band has been proposed to be of e_g character⁷⁸. These facts strongly question the validity of a pure t_{2g} model for the description of the low-energy spectra. We nevertheless present both, a t_{2g} and d - dp model, for the sake of comparison with work done in the literature and assessing trends along the perovskite series.

C. Hubbard parameters within the d - dp Hamiltonian

We first consider the d - dp low-energy Hamiltonian for the $3d$ series. The Slater integrals (Appendix B, Eq. 35) for the screened interactions, F^k , and for the bare interactions, F_{bare}^k are collected in Table II. The monopole part, F^0 , is more efficiently screened than the multipole parts, (F^2, F^4) ^{15,22,81}. The bare ratio $F^4/F^2|_{\text{bare}}$ is close to the atomic value around 0.63. In contrast, the partially screened ratio F^4/F^2 deviates from this limit. This illustrates the importance of calculating the *whole set of three* Slater integrals for accurately parametrizing the four-index Hubbard interaction matrix, rather than deducing F^0 , $(F^2 + F^4)/14$ from two independent relations and then assuming $F^4/F^2 = 0.63$ as a third one.

The Slater integrals can still be used in order to deduce effective interactions between t_{2g} orbitals (from Eq. 27 to Eq. 29). The values of these interactions are shown in Table II. The validity of the Slater parametrization can be assessed by comparing these values to the ones obtained from a direct calculation with cubic symmetry (Appendix C). For SrVO_3 , the direct calculation gives for the intra- t_{2g} interaction $U_{mm} = 4.0$ eV and $J_m = 0.60$ eV, hence in reasonable agreement with the values calculated from the Slater integrals in Tab. II. For the SrMO_3 series below, we will hence refer either to U_{mm} , J_m or \bar{U}_{mm} , \bar{J}_m .

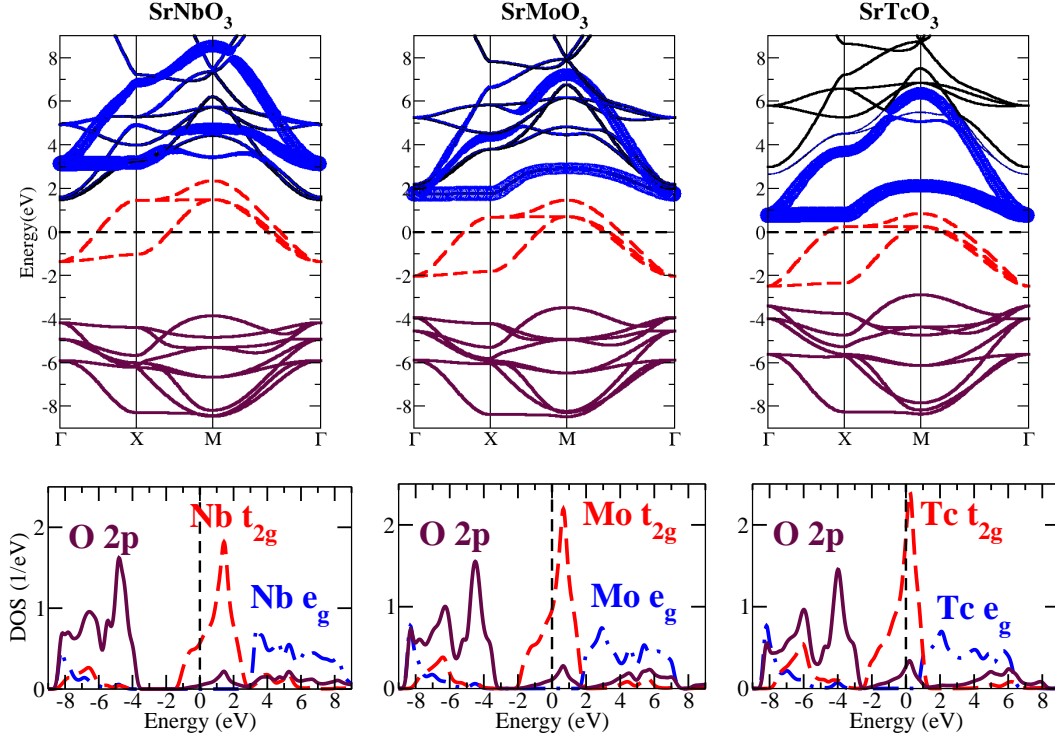


Figure 2: (color online) DFT-LDA paramagnetic eigenstates (top) and partial density of states (middle) of SrMO_3 ($M = \text{Nb}, \text{Mo}, \text{Tc}$ from left to right). $4d$ t_{2g} states are highlighted in purple, $4d$ e_g in blue and oxygen $2p$ in maroon. For comparison, the density of states of the $3d$ isoelectronic and isostructural analogues (bottom) are also shown. The LDA p - d charge transfer is bigger in $4d$ than in $3d$ perovskites.

In Fig. 3, the t_{2g} interactions for the bare, partially and fully screened cases, are shown. Along the $3d$ series, the bare interactions v_{mm} and J_m^{bare} increase with the number of electrons in the d manifold. This is due to the increasing localization of the Wannier d orbitals from SrVO_3 to SrMnO_3 within the downfolded d - dp Hamiltonian. A similar behavior is expected for hydrogenoid systems within the Slater rules, for which the atomic d radial extension decreases from V^{4+} to Mn^{4+} . The less extended the orbitals, the higher the Coulomb repulsion.

The effective interactions, U_{mm} and W_{mm} , differs from the bare interaction v_{mm} because of the screening that arises from the electronic polarizability and lowers the Coulomb repulsion. Interestingly, W_{mm} decreases with the atomic number as a consequence of increasing screening. Screening therefore counteracts the trend of increasing orbital localization that tends to increase the interaction matrix elements towards the end of the $3d$ series. The ratio W_{mm}/v_{mm} quantifies the increase of the screening from SrVO_3 to SrMnO_3 . The smaller this ratio the stronger is the screening. We obtain 6.7/100 in SrVO_3 , 4.6/100 in SrCrO_3 and 4/100 in SrMnO_3 .

Electronic screening is mediated by the creation of particle-hole and plasma excitations. At the RPA level, its strength varies with the inverse of the energy difference between occupied and empty states. The knowledge of the DFT-LDA band structure (Fig. 1) thus allows us

to analyse the efficiency of the different screening channels. The charge transfer energy between the oxygen p and the transition metal d states decreases from SrVO_3 to SrMnO_3 . The Kohn-Sham states with ligand p character go up toward the t_{2g} ones. Furthermore, the crystal field splitting to the e_g states decreases. While the absolute magnitude of the energy difference between p - and e_g - states may depend on the approximation used in the band calculation (and in particular, is slightly underestimated in the LDA), the overall trend is not an artifact of DFT-LDA^{1,60}. Experimentally, it has been evidenced e.g. in optical measurements⁵⁹. As a consequence, dd and pd screening channels give stronger contributions in SrMnO_3 than in SrVO_3 . However, these screening channels are only part of the multiple screening channels that contribute to the reduction of the Coulomb repulsion from v_{mm} to W_{mm} . For example in SrVO_3 , $v_{mm} = 20.7$ eV whereas $W_{mm} = 1.4$ eV. As already pointed out in Ref. [39], the effects of the screening channels are not additive. Nevertheless, their contribution to the total polarizability can be estimated by evaluating partially screened interactions.

The evaluation of the quantity U_{mm}/v_{mm} and the comparison with W_{mm}/v_{mm} , quantify the weight of the dd transitions in the total polarization. For example in SrVO_3 , U_{mm}/v_{mm} equals 19.8/100 whereas W_{mm}/v_{mm} equals 6.7/100. In SrCrO_3 , $U_{mm}/v_{mm} =$

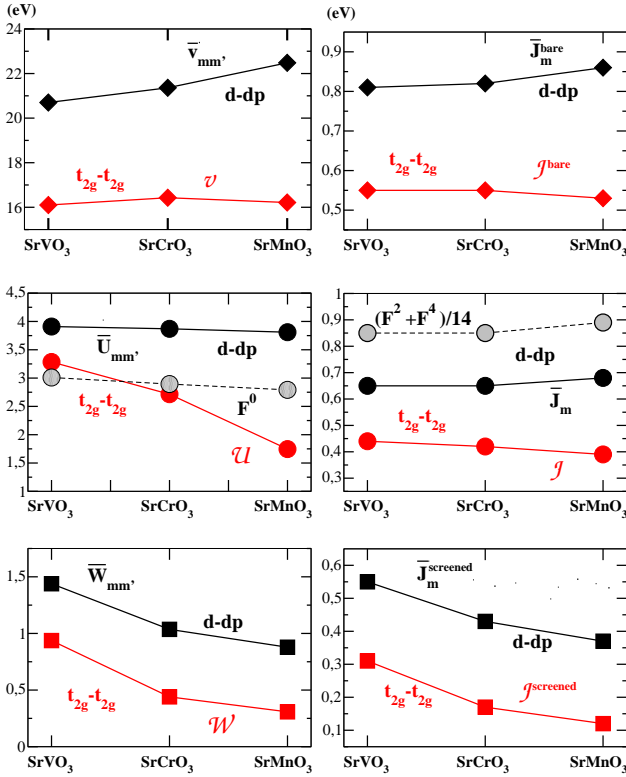


Figure 3: (color online) Middle panel: On-site Hubbard interaction \bar{U}_{mm} (left) and exchange interaction \bar{J}_{mm} (right) between t_{2g} orbitals within the d - dp (black curve) low-energy Hamiltonians for 3d SrMO₃, compared to the on-site \mathcal{U} and \mathcal{J} within t_{2g} - t_{2g} (red curve). In dashed line with open circles, the Hubbard parameter $U = F^0$ and Hund's exchange $J = (F^2 + F^4)/14$ are shown. Top panel: Same but for the bare interactions between t_{2g} orbitals. Bottom panel: Same but for the fully screened interactions between t_{2g} orbitals.

18.2/100 and $W_{mm}/v_{mm} = 4.6/100$, while in SrMnO₃, $U_{mm}/v_{mm} = 16.9/100$ and $W_{mm}/v_{mm} = 4.0/100$. The partial screening *without the dd channels*, increases more slowly through the early 3d TM oxides than the total screening. The interactions U_{mm} thus correspond to an intermediate situation between v_{mm} and W_{mm} , where the increase in partial screening counterbalances the increasing localization of the orbitals. As a result, even though W_{mm} decreases and v_{mm} increases with the atomic number, U_{mm} depends barely on it.

The values of U_{mm} indicate how strong the contribution of the dd screening channels is to the total polarizability. These channels are only partly responsible for the screening that reduces v_{mm} . The role of the pd screening channels can also be estimated. By computing the partially screened interaction after the elimination of all pd transitions (as well as dd), one gets 11 eV in SrVO₃, 10.8 eV for SrCrO₃ and 10.7 eV for SrMnO₃. Screening without these channels has thus reduced the interaction by roughly a factor two, compared to the bare interaction

v_{mm} . Low-energy screening channels, such as dd or pd , are thus responsible for about half of the total screening. On the other side, the transitions at higher energies also participate to the total polarizability leading to the strong reduction of the bare Coulomb repulsion.

Hund's exchange J is deduced from the Slater integrals F^2 and F^4 (Tab. II). In the 3d SrMO₃ series, J goes from about 0.8 eV to $J_{bare} \approx 1.0$ eV. The corresponding exchange interaction between t_{2g} , $J_m \approx 0.6 - 0.7$ eV, is smaller than J and the values agree with the ones usually employed in models for such oxides.

The fully screened exchange interaction $J_m^{screened}$, calculated from the total polarization, can be evaluated for the series. $J_m^{screened}$ slightly decreases with the d electron number in contrast to the unscreened Hund's exchange J_m^{bare} . Cutting off transitions from and to the d Kohn-Sham bands within $\mathbb{W}_{t_{2g}}$, J_m still increases from SrVO₃ to SrMnO₃. In contrast to U_{mm} , J_m hence reproduces the atomic-like trend. The weaker dependence of the exchange interactions on the screening results in J_m varying in a similar way as J_m^{bare} .

D. Hubbard parameters within the t_{2g} - t_{2g} Hamiltonian

Within the t_{2g} - t_{2g} Hamiltonian, the t_{2g} -projected local orbitals within the energy window $\mathbb{W}_{t_{2g}}$ (Tab. I) lead to "extended" t_{2g} Wannier orbitals. The charge transfer energy and the hybridization between the t_{2g} and the oxygen ligand p bands, are responsible for the finite weight of the t_{2g} Wannier functions on the oxygen atomic sites. The tail and hence the extension of the so constructed local orbitals, increases when the pd charge transfer energy becomes smaller, as happens for the 3d SrMO₃ series.

The t_{2g} local orbitals are hence more extended in SrMnO₃ than in SrVO₃, in contrast to the atomic orbitals. It implies that i) the unscreened interaction \mathcal{V} within the t_{2g} - t_{2g} model does not increase with the atomic number as v_{mm} in the previous d - dp model (Fig. 3 and Tab. II) and ii) the values of \mathcal{V} are smaller than the values of v_{mm} within d - dp .

The interaction values that would be appropriate for the t_{2g} -restricted Hubbard Hamiltonian are given in Tab. III. Their evolution along the series is illustrated in Fig. 3. A comparison with the cRPA values from the literature but with different frameworks for constructing t_{2g} local orbitals, is in order here: In SrVO₃, Aryasetiawan and co-workers³⁹ report $\mathcal{U} = 3.5$ eV within the head of LMTO's, while Miyake and Aryasetiawan³⁶ give $\mathcal{U} = 3.0$ eV, $\mathcal{J} = 0.43$ eV within MLWF. We obtain $\mathcal{U} = 3.2$ eV and $\mathcal{J} = 0.46$ eV.

We now turn to the values through the early series of the 3d TM oxides. \mathcal{U} significantly lessens from SrVO₃ to SrMnO₃ and the decrease of \mathcal{U} is more pronounced than U_{mm} within the d - dp model. The decrease of \mathcal{U} is still due to the screening which gets larger with the atomic number. More precisely, the $p \rightarrow t_{2g}$ and $t_{2g} \rightarrow$

Table III: Hubbard-Kanamori \mathcal{U} , bare \mathcal{V} and fully screened \mathcal{W} interactions and corresponding exchange interactions, \mathcal{J} , $\mathcal{J}_{\text{bare}}$ and $\mathcal{J}_{\text{screened}}$ between t_{2g} orbitals within the t_{2g} - t_{2g} downfolded Hamiltonian for the early $3d$ series SrMO_3 ($M = \text{V, Cr, Mn}$) and $4d$ ($M = \text{Nb, Mo, Tc}$). The inter-orbital interactions \mathcal{U}' coincide with $\mathcal{U} - 2\mathcal{J}$.

(eV)	V	Cr	Mn	Nb	Mo	Tc
\mathcal{U}	3.2	2.7	1.8	3.0	3.0	2.9
\mathcal{J}	0.44	0.42	0.39	0.29	0.31	0.31
\mathcal{V}	16.1	16.4	16.2	10.7	11.6	11.8
$\mathcal{J}_{\text{bare}}$	0.55	0.55	0.53	0.38	0.40	0.39
\mathcal{W}	0.9	0.4	0.3	0.9	0.5	0.4
$\mathcal{J}_{\text{screened}}$	0.30	0.17	0.12	0.24	0.19	0.16
$\mathcal{U}/\mathcal{V} \times 100$	19.8	16.4	11.1	28	25.8	24.6
$\mathcal{W}/\mathcal{V} \times 100$	5.6	2.4	1.8	8.4	4.3	3.4

e_g channels contribute more and more to the screening from SrVO_3 to SrMnO_3 , because of the p and e_g Kohn-Sham bands that go closer and closer to the Fermi level. Quantitatively, the ratio \mathcal{U}/\mathcal{V} is about twice larger in SrVO_3 than in SrMnO_3 (Tab. III). The fully screened interactions, \mathcal{W} , on the other hand, decrease through the series.

In contrast to J_m and J_m^{bare} within the d - dp model, the exchange interactions, \mathcal{J} and $\mathcal{J}_{\text{bare}}$ within the t_{2g} - t_{2g} model slightly decrease with the number of d electrons. Considering the total polarization leads to a significant decrease of $\mathcal{J}_{\text{screened}}$ through the series. Since the reduction is weaker for \mathcal{J} than for $\mathcal{J}_{\text{screened}}$, the screening induced by the $t_{2g}t_{2g}$ transitions must be responsible for the behavior of $\mathcal{J}_{\text{screened}}$. As \mathcal{U} , the exchange interactions therefore depend on the extension of the local orbitals: \mathcal{J} is smaller within the t_{2g} - t_{2g} Hamiltonian than J_m within d - dp .

E. $4d$ perovskites: experimental facts

We now turn to the $4d$ series SrMO_3 ($M = \text{Nb, Mo, Tc}$). The lattice parameters used in the calculations are summarized in Table I.

SrNbO₃: This compound is usually obtained with a non-stoichiometric perovskite structure⁸². When doping into Sr_xNbO_3 with $x > 0.80$, a cubic perovskite phase is observed exhibiting a poor paramagnetic metallic behavior at temperatures below 300 K⁸³.

SrMoO₃: It is, in contrast, an excellent paramagnetic metal- even the $4d$ transition metal oxide that displays the highest electrical conductivity⁸⁴. With two electrons on the t_{2g} shell, it is an electronic analogue of SrRuO_3 that has two holes on the t_{2g} 's but larger correlation effects due to the Van Hove singularity found in its density of states⁴⁴.

SrTcO₃: Because of the radioactivity of technetium,

this compound has been less studied, and only structural and magnetic properties are known. A huge Néel temperature of 1023 K – accompanied by a G-type antiferromagnetic ordering with the magnetic moment $2.1\mu_B$ below T_N – has been recently discovered⁸⁵. In particular, this high T_N is larger than in the $3d$ analogue SrMnO_3 . The large T_N in SrTcO_3 was first interpreted within density functional calculations^{85–87}, e.g. in terms of the larger covalency of the Tc-O bonding compared to Mn-O⁸⁵. Recently, another scenario has been put forward for interpreting the difference of magnitude in T_N between SrTcO_3 and SrMnO_3 , based on the proximity of SrTcO_3 to the Mott transition in the presence of large Hund's exchange at half-filling⁸⁸.

F. Hubbard interactions in $4d$ perovskites

In the $4d$ SrMO_3 series, the evolution of the Kohn-Sham bands from Nb to Tc oxides is analogous to the one in the isoelectronic and isostructural $3d$ compounds, but the trends are less pronounced (Fig. 2). The pd charge transfer energy decreases more slowly in the $4d$ series, and so do the crystal and ligand fields that split the t_{2g} and e_g bands. As a result, the transition metal e_g states overlap with strontium $5s/4d$. For this reason, only the t_{2g} Hamiltonian is considered here.

The atomic-like character of the t_{2g} Wannier basis is evidenced by the atomic-like behavior of the bare interaction \mathcal{V} in the $4d$ series (Fig. 4): \mathcal{V} becomes larger with the atomic number, as in $3d$ when considering the d - dp Hamiltonian. The local basis designed for the t_{2g} degrees of freedom, is atomic-like for $4d$ oxides in contrast to the one for t_{2g} in $3d$. The difference in $4d$ comes from the larger charge transfer energy which leads to a smaller tail of the downfolded orbital with t_{2g} character on the oxygen sites.

However, the orbital extension of the t_{2g} local orbitals has to be larger in $4d$ than in $3d$ oxides since the bare interaction \mathcal{V} are twice smaller in the former (Tab. III). This makes sense in an atomic-like basis in which the extension of the $4d$ atomic wavefunctions is larger than the extension of $3d$.

Since the pd charge transfer energy as well as the t_{2g} - e_g splitting decrease slower in $4d$ oxides, the pd and the $t_{2g}e_g$ channels are not as efficient in screening as in the $3d$ analogues. This is quantitatively highlighted by the ratios \mathcal{U}/\mathcal{W} (Tab III), which are larger in $4d$ and decrease slower through the $4d$ series.

Consequently, \mathcal{U} in $4d$ is almost constant with the d electron number, like U_{mm} in the d - dp model for $3d$ TM oxides, whereas \mathcal{U} in $3d$ significantly lessens until becoming smaller in SrMnO_3 than in SrTcO_3 (Fig. 4). This is an effect of the screening which has stronger impact in the $3d$ extended Wannier basis than in the atomic-like $4d$ one.

The exchange interactions in $4d$ oxides behave in a similar way as in $3d$ (Tab. III). The exchange interactions

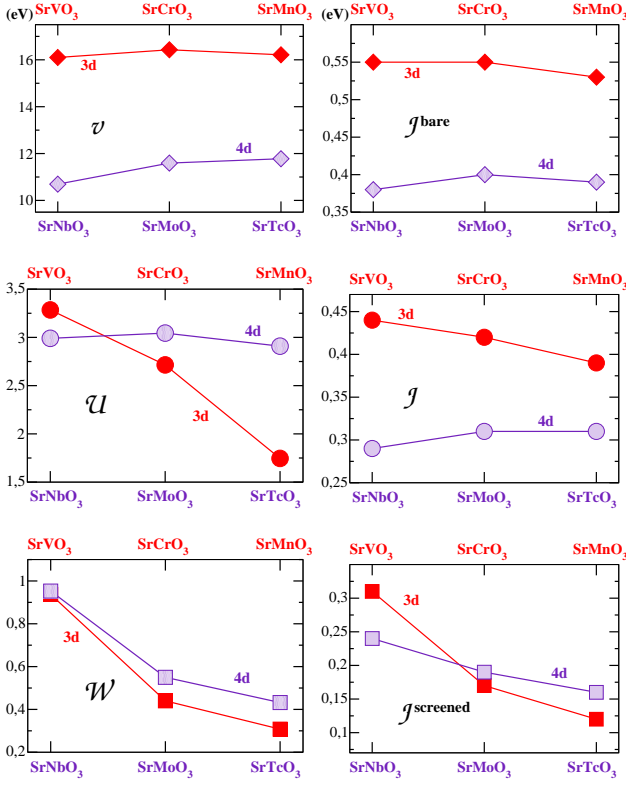


Figure 4: (color online) Middle panel: On-site Hubbard-Kanamori interaction U (left) and exchange interaction J (right) between t_{2g} orbitals within the t_{2g} - t_{2g} low-energy Hamiltonian for 3d (red curve) and 4d (indigo curve) SrMO_3 (see also Tab. III). Top panel: Same but for the bare interaction V and J_{bare} between t_{2g} orbitals. Bottom panel: Same but for the fully screened interaction W and J_{screened} between t_{2g} orbitals.

in 4d are about 0.1 eV smaller than in 3d. This is due to the higher extension of the 4d Wannier orbitals which is also responsible for the smaller bare interactions V .

G. The influences of structural distortions: the example of SrMnO_3

At room temperature, SrMnO_3 crystallises in the four-layers hexagonal structure ($P63/mmc$) with $a = 5.461 \text{ \AA}$, $c = 9.093 \text{ \AA}$ ⁷⁴. The DFT-LDA band structure is shown in Fig. 5.

The four-times larger unit cell leads to a backfolding of bands in the first Brillouin zone. A set of t_{2g} -like bands (Fig. 5) can be identified with the twelve bands around the Fermi level and a set of e_g -like bands with the eight ones above. A d - dp model is constructed rather than a t_{2g} one. This allows for a direct comparison of the Slater integrals (Eq. 35) calculated within the d - dp model built for the cubic crystal structure (Tab. IV).

U as well as v are slightly bigger in the hexagonal phase

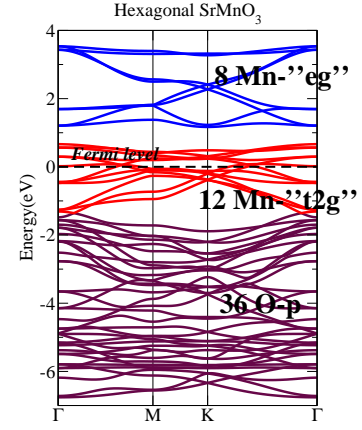


Figure 5: (color online) DFT-LDA band structure of the four-layers hexagonal unit cell of SrMnO_3 in the paramagnetic phase. Lattice parameters $a = 5.461 \text{ \AA}$, $c = 9.093 \text{ \AA}$ are taken from⁷⁴.

Table IV: Screened and bare Slater integrals for the d - dp model in cubic and hexagonal SrMnO_3 .

(eV)	F^0	F^4/F^2	J	F^0_{bare}	$F^4/F^2 _{\text{bare}}$	J_{bare}
cubic	2.8	0.774	0.9	21.2	0.625	1.1
hexagonal	3.1	0.777	0.9	21.9	0.621	1.1

than in the cubic one. This is an effect of the Wannier orbital localization rather than a screening effect since also the bare interaction v is enhanced. Hund's exchange J does not change much between the two crystal structures.

V. HUBBARD INTERACTIONS IN THE LAYERED PEROVSKITE OXIDES Sr_2MO_4 ($M = \text{MO, TC, RU, RH}$)

A. General features

The second class of oxides that we have investigated are the layered perovskites Sr_2MO_4 ($M = \text{Mo, Tc, Ru, Rh}$) where M^{4+} is a 4d transition metal. The lattice parameters used in the electronic structure calculations for the paramagnetic phase are given in Table V.

Sr_2MoO_4 : This compound exhibits a metallic behavior over a wide range of temperature between 80 mK and 300 K, with a resistivity increasing between 2 and 10 $\text{m}\Omega\cdot\text{cm}$ ⁸⁹. It is usually investigated under the possibility that it could exhibit analogous electronic properties than Sr_2RuO_4 , although a superconducting state has not been reported down to 25 mK.

Sr_2TcO_4 : Due to the radioactivity of technetium elements, only structural properties are known for Sr_2TcO_4 . An undistorted layered perovskite structure is considered below.

Table V: Lattice parameters used for the layered Sr_2MO_4 perovskites and energy windows \mathbb{W} (in eV) for the d - dp and t_{2g} - t_{2g} models.

	a (Å)	c (Å)	\mathbb{W}_{dp}	$\mathbb{W}_{t_{2g}}$
Sr_2MoO_4	3.917	12.859	$[-10, 8.5]$	$[-2.0, 2.0]$
Sr_2TcO_4	3.902	12.720	$[-10, 7.5]$	$[-2.6, 1.3]$
Sr_2RuO_4	3.863	12.724	$[-10, 6.9]$	$[-3.0, 1.0]$
Sr_2RhO_4	3.854	12.880	$[-10, 6.0]$	$[-3.3, 0.5]$

Sr_2RuO_4 : The resistivity of this compound obeys a T^2 law below 30 K, evidencing a Fermi liquid behavior. A strong anisotropy of the transport properties – due to its layered structure – was reported⁹⁰. A large mass enhancement and a low coherence scale have been determined experimentally. Sr_2RuO_4 also exhibits an unconventional superconductivity below 2 K⁹¹. The three-sheet Fermi surface determined experimentally is reasonably well described by DFT-LDA calculations, but the enhancement and the anisotropy in the mass are missed. The largest mass enhancement surprisingly appears for the widest d_{xy} band as determined by quantum oscillations experiments⁹¹. Several LDA+DMFT calculations have been carried out to reproduce the low-energy properties of the photoemission spectra^{44,92–94}.

Sr_2RhO_4 : The symmetry is lowered from the K_2NiF_4 class by 11° rotation around the c -axis of the RhO_6 octahedra⁹⁵. It is a paramagnetic metal down to 36 mK⁹⁶. Spin-orbit coupling (SOC) was found to be relevant in addition to electronic correlations^{97–99}. LDA+DMFT calculations with SOC have been recently performed for the distorted structure and compared to the isoelectronic but Mott insulating Sr_2IrO_4 ⁴⁵. In particular, it was shown how the interplay of SOC, correlations and structural distortions leads to a suppress of the effective orbital degeneracy, leaving only two orbitals at the Fermi level. In the following, for computational reasons, the undistorted crystal structure of Sr_2RhO_4 is considered.

The DFT-LDA band structures for the paramagnetic phases are shown in Fig. 6. Bands with (d_{xy}, d_{xz}, d_{yz}) orbital character emerge around the Fermi level, whereas the $(d_{3z^2-r^2}, d_{x^2-y^2})$ orbital character is found above and the oxygen p 's lie below. The band with d_{xy} character leads to a quasi-two dimensional Fermi surface whereas the degenerate bands with (d_{xz}, d_{yz}) character give rise to a quasi-one dimensional Fermi surface. In Sr_2MO_4 and Sr_2TcO_4 , the e_g states are entangled with the strontium-like d 's but come closer to the t_{2g} 's when the $4d$ electron number increases. On the other hand, the pd charge transfer energy decreases with this number, since the p 's go up toward the Fermi level. This decrease makes larger the screening from the p channels, in an analogous way to in the early transition metal oxide series.

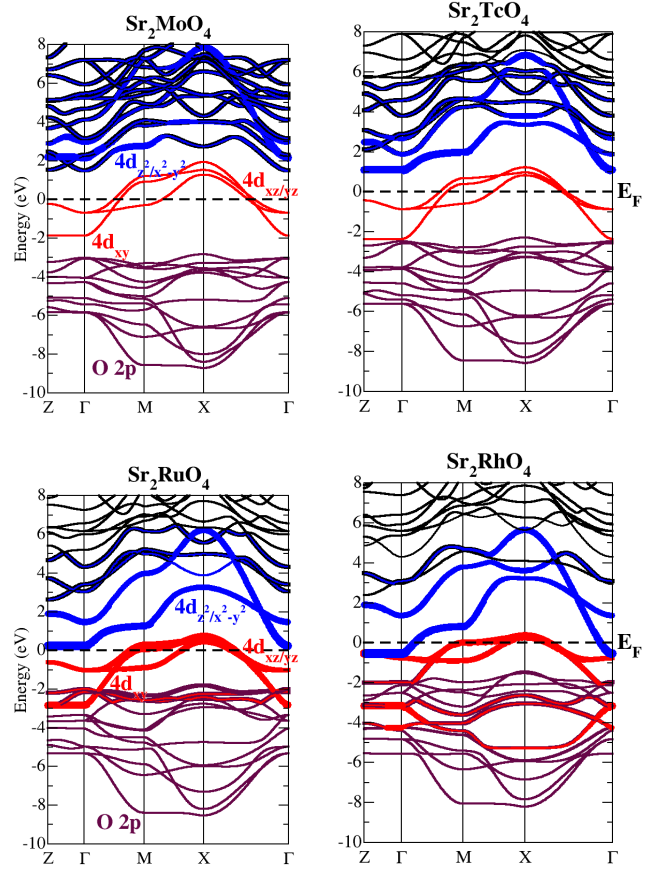


Figure 6: (color online) DFT-LDA paramagnetic band structures for layered perovskites Sr_2MO_4 . (top): From left to right: $M = \text{Mo}, \text{Tc}$. (bottom): From left to right: $M = \text{Ru}, \text{Rh}$.

B. Hubbard parameters within the d - dp Hamiltonian

As previously, also for the early TM oxides within the layered perovskite structure Sr_2MO_4 , we consider first the d - dp Hamiltonian. The $4d$ Wannier orbitals are constructed out of the Kohn-Sham bands within the energy window \mathbb{W}_{dp} (Tab. V).

The Slater integrals are given in Tab. VI. The value of the ratio $F^4/F^2|_{\text{bare}}$ is close to the one calculated for $4d$ atoms¹⁰⁰. A significant deviation is obtained for the screened ratio of the Slater integrals, which is even stronger than the one in the $3d$ SrMO_3 series. This seems natural, given the anisotropy of the structure and the screening which increases with the orbital extension.

A cubic approximation can be used for deducing a set of interactions between (d_{xy}, d_{xz}, d_{yz}) local orbitals from the Slater integrals (Eqs. 27, 28 and 29). The values are shown in Tab. VI and can be compared to the matrix elements calculated directly (Tab. VII and see also Appendix D). The latter are anisotropic within the plane of the TM and oxygen octahedra. The Slater parametriza-

Table VI: (top) Static and bare Slater integrals for the d - dp Hamiltonian in $4d$ Sr_2MO_4 . (bottom) Slater-symmetrized effective interactions between t_{2g} orbitals.

(eV)	F^0	F^4/F^2	J	F^0_{bare}	$F^4/F^2 _{\text{bare}}$	J_{bare}
Mo	3.26	0.862	0.67	14.50	0.684	0.86
Tc	3.19	0.850	0.70	15.25	0.673	0.90
Ru	3.23	0.838	0.74	15.97	0.669	0.94
Rh	3.44	0.820	0.78	16.77	0.663	0.98
	\bar{U}_{mm}	$\bar{U}_{mm'}$	\bar{J}_m	\bar{v}_{mm}	$\bar{v}_{mm'}$	\bar{J}_m^{bare}
Mo	4.0	3.0	0.50	15.5	14.1	0.66
Tc	4.0	2.9	0.53	16.3	14.9	0.69
Ru	4.1	2.9	0.56	17.0	15.6	0.72
Rh	4.3	3.1	0.59	17.9	16.4	0.75

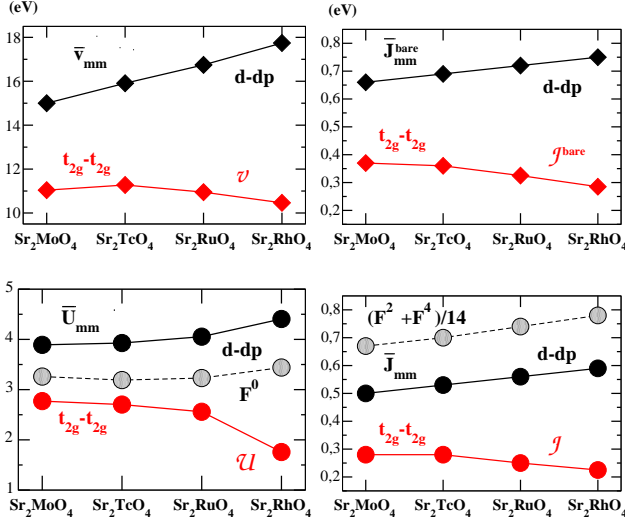


Figure 7: (color online) Bottom panel: On-site interaction U_{mm} (left) and exchange interaction J_m (right) between t_{2g} orbitals within the d - dp (black curve) model for Sr_2MO_4 and on-site interactions \mathcal{U} (left) and \mathcal{J} (right) but within t_{2g} - t_{2g} (red curve). In dashed line with open circles, the Hubbard parameter $U = F^0$ and Hund's exchange $J = (F^2 + F^4)/14$ are shown. Top panel: Same but for the bare interactions between the t_{2g} orbitals.

tion is more accurate for the late materials, Sr_2TcO_4 and Sr_2RhO_4 , for which the spherical approximation of the $4d$ orbital is better due to the smaller hybridization with the ligands.

The bare on-site and exchange interactions increase with the number of the $4d$ electrons (Fig. 7), suggesting a rather atomic-like behavior of the $4d$ Wannier orbitals within the d - dp Hamiltonian. This agrees with the atomic expectations based on the Slater rules, *ie* a higher localization due to the contraction of the atomic $4d$ wavefunction from the left to the right of the periodic classification.

In the d - dp model, the dd transitions are removed from

Table VII: Hubbard-Kanamori parameters $\mathcal{U}, \mathcal{U}', \mathcal{J}$ for the t_{2g} - t_{2g} model and average interactions between the t_{2g} orbitals within d - dp in Sr_2MO_4 . The ratios \mathcal{U}/\mathcal{V} in t_{2g} - t_{2g} and U_{mm}/v_{mm} in d - dp have been multiplied by a factor 100.

	t_{2g} - t_{2g}				d - dp		
(eV)	\mathcal{U}	\mathcal{U}'	\mathcal{J}	\mathcal{U}/\mathcal{V}	U_{mm}	J_m	U_{mm}/v_{mm}
Mo	2.77	2.15	0.28	24.8	3.8	0.48	25.3
Tc	2.70	2.07	0.28	24.3	3.9	0.52	24.5
Ru	2.56	1.94	0.26	23.2	4.0	0.55	23.9
Rh	1.76	1.18	0.23	16.6	4.4	0.61	24.8

the screening in order to obtain the Hubbard interaction matrices (Tab. VI and Appendix D). As the bare interaction, the on-site Hubbard interaction gets larger with the $4d$ electron number (Fig. 7). This is rationalized by the fact that the screening only slightly increases from Sr_2MoO_4 to Sr_2RhO_4 as indicated by the small decrease of the ratio U_{mm}/v_{mm} (Tab. VII), from 25.8/100 to 24.8/100. The increase of the screening is thus not able to counterbalance the effects due to the stronger orbital localization.

The Hund's exchange interaction (Fig. 7) also reproduces the atomic trend, increasing with the atomic number.

C. Hubbard parameters within the t_{2g} - t_{2g} Hamiltonian

Alternatively, one can construct the low-energy Hamiltonian that only includes the (d_{xy}, d_{xz}, d_{yz}) degrees of freedom. The energy windows $\mathbb{W}_{t_{2g}}$ are given in Tab. V.

Since the pd charge transfer energy decreases throughout the series, the tail on the oxygen atomic sites of the downfolded local orbitals gets larger from Sr_2MoO_4 to Sr_2RhO_4 . Consequently, the orbital localization decreases with the $4d$ electron number, in contrast to the atomic d wavefunctions. The trends for the bare interactions thus deviate from the atomic ones, which were previously reported for the d - dp model (Fig. 7 and Tab. VII).

The orbitally-resolved interactions (see Appendix D) calculated within the t_{2g} - t_{2g} Hamiltonian are more anisotropic than their analogues within the d - dp Hamiltonian. This is another signature of the less spherical character of the downfolded orbitals within t_{2g} - t_{2g} . The largest interactions are interestingly obtained on the d_{xy} local orbital, for both the screened and bare cases.

The on-site t_{2g} interaction \mathcal{U} and Hund's exchange \mathcal{J} exhibit trends that are similar to \mathcal{V} and J_{bare} (Fig. 7). The decrease from Sr_2MoO_4 to Sr_2RhO_4 is even more pronounced. This is due to the screening which strongly and non-linearly increases between Sr_2RuO_4 and Sr_2RhO_4 . Indeed, the ratio \mathcal{U}/\mathcal{V} within the t_{2g} - t_{2g} model (Tab. VII) is divided by almost a factor two through the series, whereas the ratio U_{mm}/v_{mm} is slowly decreasing within the d - dp model.

The difference in the screening between the two low-energy Hamiltonians comes from the transitions between t_{2g} and e_g Kohn-Sham eigenstates, which are removed from the total polarization in the d - dp model. These transitions – by causing a notable increase of the screening between Sr_2RuO_4 and Sr_2RhO_4 – are responsible for the smaller effective interactions in the latter. Within DFT-LDA (Fig. 6), the e_g 's come closer to the Fermi level in the late Sr_2MO_4 perovskites. The e_g bands are even partially filled in Sr_2RhO_4 leading to a metallic screening that contributes to lower the effective interactions. This is an artefact of the undistorted crystal structure of Sr_2RhO_4 and is not the case for the realistic distorted structure⁴⁵.

VI. CONCLUSIONS AND OUTLOOK

Viewing the Hubbard and Hund interactions of a correlated electron material as bare interactions within a reference system with reduced number of degrees of freedom, gives these parameters the status of auxiliary quantities, only meant to represent the physical fully screened interaction W . From a conceptual point of view, they are then defined as soon as the reference system is specified. From a practical point of view, also the approximations to W and to the polarization of the reference system P^{sub} have to be chosen. The lattice version of cRPA corresponds in this language to the choice of a low-energy subsystem, and the choice of the random phase approximation for the evaluation of all polarizations.

In this work, we have presented an implementation of the constrained Random Phase Approximation in a density functional theory electronic structure code within the linearized augmented plane wave framework. The method gives access to the matrix elements of the Hubbard interaction matrix in a localized basis set of a downfolded lattice Hamiltonian. The strength of the Coulomb interactions is parametrized by the Hubbard U and Hund's exchange J , which can be used for the description of correlated electron systems within interacting lattice Hamiltonians.

We have calculated the Hubbard U and Hund's exchange J for the $3d$ and $4d$ ternary oxides SrMO_3 ($M = \text{V, Cr, Mn}$) and ($M = \text{Nb, Mo, Tc}$). Within a low-energy Hamiltonian (" d - dp ") that includes both d and oxygen p degrees of freedom – and an occupation energy cost on d only – U does not change much with the d electron number. We have rationalized this trend as a competition between two aspects: increasing orbital localization – as evidenced also by the increasing bare interaction v – and increasing screening due to the reduction of the charge transfer energy with the oxygen ligands – as illustrated by a decrease of the screened interaction W . An alternative low-energy Hamiltonian, based on the t_{2g} degrees of freedom only (" t_{2g} - t_{2g} "), has also been constructed. Within this framework, both U and – to a lesser extent – J decrease with the d electron number in $3d$ oxides, as

a consequence of the extended character of the localized t_{2g} orbitals. This is due to the downfolding of the tails of oxygen- p character. In $4d$ oxides, the trends for U and J are flat again, because of the larger charge transfer energy with the oxygen- p states. The surprisingly smaller U for SrMnO_3 than for SrTcO_3 within cRPA for such Hamiltonian can be understood in terms of the weaker screening effects in the latter.

We have considered analogous low-energy Hamiltonians for the materials with the layered perovskite structure Sr_2MO_4 ($M = \text{Mo, Tc, Ru, Rh}$). For the same reasons as in the ternary oxides, U and J increase with the atomic number within the d - dp Hamiltonian, while they decrease within the t_{2g} - t_{2g} Hamiltonian.

We have emphasized the dependence of the effective Coulomb interactions on the choice of the one-particle part of the Hamiltonian. Determining Hubbard U and Hund's J entirely from first principles for a given low-energy Hamiltonian opens the way to a *truly ab initio* description of correlated materials within many-body calculations.

ACKNOWLEDGMENTS

We acknowledge useful discussions with M. Aichhorn, F. Aryasetiawan, A. Georges, D. Khomskii, M. Imada, T. Miyake, J. Mravlje, L. Pourovskii, P. Rinke, G. Sawatzky, M. Scheffler, M. van Schilfhaarde and V. Vildosola. This work was supported by the French ANR under project SURMOTT and IDRIS/GENCI under project 1393, and Natural Science Foundation of China (Project No. 20973009).

While this work was being written, an alternative implementation of cRPA within a pseudopotential code was proposed in Ref. [101].

APPENDIX A : Technicalities of the cRPA implementation within the (L)APW+lo framework

We report below on the technicalities that are specific to the cRPA part. Our cRPA implementation relies on the recent GW implementation within the (L)APW+lo framework called FHI-GAP¹⁰². Details related to the construction of an optimized product mixed basis for expanding polarizations, dielectric functions and Coulomb interactions, can be found in Ref. [102]. We will hence employ the same notations as in this reference. The product mixed basis, for example, will be denoted $\{\chi_i^{\mathbf{q}}(\mathbf{r})\}$, where \mathbf{q} -vectors belong to the first Brillouin zone and i -indices run over the size of the complete product mixed basis.

The total polarization at the RPA level can be expanded into the product mixed basis $\{\chi_i^{\mathbf{q}}(\mathbf{r})\}$ ^{103,104}:

$$P(\mathbf{r}, \mathbf{r}'; \omega) = \frac{1}{N} \sum_{\mathbf{q}} \sum_{ij} [\chi_i^{\mathbf{q}}(\mathbf{r})]^* P_{ij}(\mathbf{q}, \omega) \chi_j^{\mathbf{q}}(\mathbf{r}'),$$

where the \mathbf{q} -summation (of \mathcal{N} size) is performed over the first Brillouin zone. The polarization matrix elements in the product basis, P_{ij} , read as :

$$P_{ij}(\mathbf{q}, \omega) = \frac{1}{\mathcal{N}} \sum_{\mathbf{k}} \sum_{n, n'}^{\text{occ, unocc}} M_{nn'}^i(\mathbf{k}, \mathbf{q}) F_{nn'\mathbf{k}}(\mathbf{q}, \omega) [M_{nn'}^j(\mathbf{k}, \mathbf{q})]^*,$$

where the overlap between the Bloch wavefunctions, $\psi_{\mathbf{k}n}$, and the product mixed basis functions, denoted $M_{nn'}^i(\mathbf{k}, \mathbf{q})$, is defined as follows :

$$M_{nn'}^i(\mathbf{k}, \mathbf{q}) = \int_{\Omega} d\mathbf{r} \psi_{\mathbf{k}n}(\mathbf{r}) [\chi_i^{\mathbf{q}}(\mathbf{r}) \psi_{\mathbf{k}-\mathbf{q}, n'}(\mathbf{r})]^*,$$

and :

$$\omega_{n\mathbf{k}, n'\mathbf{k}-\mathbf{q}} = \epsilon_{n'\mathbf{k}-\mathbf{q}} - \epsilon_{n\mathbf{k}}$$

$$F_{nn'\mathbf{k}}(\mathbf{q}, \omega) = \frac{1}{\omega - \omega_{n\mathbf{k}, n'\mathbf{k}-\mathbf{q}} + i\eta} - \frac{1}{\omega + \omega_{n\mathbf{k}, n'\mathbf{k}-\mathbf{q}} - i\eta}.$$

Within the assumption that the correlated subspace \mathcal{C} is unambiguously defined since the target correlated bands do not energetically overlap with the itinerant ones, it follows for the d -restricted polarization P^d (Eq. 9) expanded into the product mixed basis :

$$P_{ij}^d(\mathbf{q}, \omega) = \frac{1}{\mathcal{N}} \sum_{\mathbf{k}} \sum_{d, d'}^{\text{occ, unocc}} M_{dd'}^i(\mathbf{k}, \mathbf{q}) F_{dd'\mathbf{k}}(\mathbf{q}, \omega) [M_{dd'}^j(\mathbf{k}, \mathbf{q})]^*,$$

and hence for the constrained polarization, P^r :

$$P_{ij}^r(\mathbf{q}, \omega) = P_{ij}(\mathbf{q}, \omega) - P_{ij}^d(\mathbf{q}, \omega).$$

The total symmetrized dielectric function, ε , in the product mixed basis is defined as follows¹⁰² :

$$\begin{aligned} \varepsilon_{ij}(\mathbf{q}, \omega) &= \delta_{ij} - v_i^{\frac{1}{2}}(\mathbf{q}) P_{ij}(\mathbf{q}, \omega) v_j^{\frac{1}{2}}(\mathbf{q}) \\ &= \delta_{ij} - \frac{1}{\mathcal{N}} \sum_{\mathbf{k}} \sum_{n, n'}^{\text{occ, unocc}} v_i^{\frac{1}{2}}(\mathbf{q}) M_{nn'}^i(\mathbf{k}, \mathbf{q}) F_{nn'\mathbf{k}}(\mathbf{q}, \omega) \\ &\quad \times [v_j^{\frac{1}{2}}(\mathbf{q}) M_{nn'}^j(\mathbf{k}, \mathbf{q})]^*. \end{aligned}$$

Analogously, the d -constrained (partial) dielectric function, ε^r , reads as

$$\varepsilon_{ij}^r(\mathbf{q}, \omega) = \delta_{ij} - v_i^{\frac{1}{2}}(\mathbf{q}) P_{ij}^r(\mathbf{q}, \omega) v_j^{\frac{1}{2}}(\mathbf{q}).$$

From the Dyson-like equation for the screened interaction (Eq. 5), it follows for W, W^r expanded into the product mixed basis :

$$\begin{aligned} W_{ij}(\mathbf{q}, \omega) &= v_i^{\frac{1}{2}}(\mathbf{q}) \varepsilon_{ij}^{-1}(\mathbf{q}, \omega) v_j^{\frac{1}{2}}(\mathbf{q}) \\ W_{ij}^r(\mathbf{q}, \omega) &= v_i^{\frac{1}{2}}(\mathbf{q}) [\varepsilon^r(\mathbf{q}, \omega)]_{ij}^{-1} v_j^{\frac{1}{2}}(\mathbf{q}). \end{aligned}$$

The product Kohn-Sham representation of W^r (Eq. 16) can be expanded into the product mixed basis via the overlap quantities $M_{nn'}^i(\mathbf{k}, \mathbf{q})$:

$$\begin{aligned} \langle \psi_{\mathbf{k}_1 n_1} \psi_{\mathbf{k}_2 n_2} | W^r | \psi_{\mathbf{k}_3 n_3} \psi_{\mathbf{k}_4 n_4} \rangle &= \frac{1}{\mathcal{N}} \sum_{\mathbf{q}} \sum_{ij} [M_{n_1 n_3}^i(\mathbf{k}_1, \mathbf{q})]^* \\ &\quad \times W_{ij}^r(\mathbf{q}, \omega) M_{n_4 n_2}^j(\mathbf{k}_4, \mathbf{q}) \delta_{\mathbf{k}_3, \mathbf{k}_1 - \mathbf{q}} \delta_{\mathbf{k}_2, \mathbf{k}_4 - \mathbf{q}}. \end{aligned}$$

and therefore, it follows for the Hubbard interactions :

$$\begin{aligned} U_{L_1 L_2 L_3 L_4}^{\mathbf{R}_1 \mathbf{R}_2 \mathbf{R}_3 \mathbf{R}_4}(\omega) &= \frac{1}{\mathcal{N}} \sum_{\mathbf{q}} e^{i\mathbf{q} \cdot (\mathbf{R}_3 - \mathbf{R}_2)} \sum_{ij} [M_{L_1 \mathbf{R}_1, L_3 \mathbf{R}_3}^i(\mathbf{q})]^* \\ &\quad \times W_{ij}^r(\mathbf{q}, \omega) M_{L_4 \mathbf{R}_4, L_2 \mathbf{R}_2}^j(\mathbf{q}), \end{aligned}$$

where $M_{L\mathbf{R}, L'\mathbf{R}'}^i(\mathbf{q})$ are defined as follows :

$$\begin{aligned} M_{L\mathbf{R}, L'\mathbf{R}'}^i(\mathbf{q}) &= \frac{1}{\mathcal{N}} \sum_{\mathbf{k}} e^{-i\mathbf{k} \cdot (\mathbf{R} - \mathbf{R}')} \\ &\quad \times \sum_{n, n' \in \mathbb{W}} [P_{Ln}(\mathbf{k},)]^* M_{nn'}^i(\mathbf{k}, \mathbf{q}) P_{L'n'}(\mathbf{k} - \mathbf{q}). \end{aligned}$$

APPENDIX B : Parametrization of the Hubbard interaction matrix with Slater integrals

The interaction matrix in atoms can be efficiently parametrized by a finite number of Slater integrals^{23,24,57} thanks to the atomic sphericity. Such parametrization can be extended to solids if one assumes that within the solid :

$$U_{m_1 m_2 m_3 m_4}^{(\text{spheric})} = \sum_{k=0}^{2l} \alpha_k(m_1, m_2, m_3, m_4) F^k, \quad (33)$$

where the angular part is described with Racah-Wigner coefficients. $\alpha_k(m_1, m_2, m_3, m_4)$ are calculated with spherical harmonics, Y_{lm} , as follows :

$$\begin{aligned} \alpha_k(m_1, m_2, m_3, m_4) &= \frac{4\pi}{2k+1} \sum_{q=-k}^k \langle Y_{l m_1} | Y_{k q} Y_{l m_3} \rangle \\ &\quad \times \langle Y_{l m_2} Y_{k q} | Y_{l m_4} \rangle, \end{aligned} \quad (34)$$

($\langle Y_{l_1 m_1} | Y_{l_2 m_2} Y_{l_3 m_3} \rangle$ corresponds to the Gaunt coefficient calculated with spherical harmonics), whereas the radial part is expressed in terms of Slater integrals $\{F^k\}$. These Slater integrals are deduced from the interaction matrix elements computed by cRPA in the Wannier basis, $\{\phi_{m, -2 \leq m \leq 2}\}$ that is said “spheric” because of its complex representation⁵¹:

$$\begin{aligned} F^k(\omega) &= \mathcal{C}_{l,k} \sum_{m_1, m_2, m_3, m_4} (-1)^{m_1 + m_4} U_{m_1 m_2 m_3 m_4}^{(\text{spheric})}(\omega) \\ &\quad \times \begin{pmatrix} l & k & l \\ -m_1 & m_1 - m_3 & m_3 \end{pmatrix} \begin{pmatrix} l & k & l \\ -m_2 & m_2 - m_4 & m_4 \end{pmatrix}, \end{aligned} \quad (35)$$

where the parentheses correspond to the Wigner 3j-symbols and the coefficients $\mathcal{C}_{l,k}$ are defined as follows :

$$\mathcal{C}_{l,k} = \frac{2k+1}{(2l+1)^2} \begin{pmatrix} l & k & l \\ 0 & 0 & 0 \end{pmatrix}^2. \quad (36)$$

The frequency dependence of the Slater integrals arises from the frequency dependence of the interaction matrix elements induced by the dynamical screening.

APPENDIX C : Reduced interaction matrices for SrMO_3 ($M = \text{V, Cr, Mn}$)

We give below the reduced interaction matrices (Eqs. 19, 20 and 21) within the d - dp model (see Tab. I for the choice of the energy windows used to construct the d Wannier orbitals) and calculated with cubic symmetry. In the following, the ordering of the orbitals in these matrices is $d_{z^2}, d_{x^2-y^2}, d_{xy}, d_{xz}, d_{yz}$. The values are given in eV.

SrVO_3

$$U_{mm'}^{\sigma\bar{\sigma}} = \begin{pmatrix} 4.43 & 2.88 & 2.73 & 3.19 & 3.19 \\ 2.88 & 4.43 & 3.35 & 2.88 & 2.88 \\ 2.73 & 3.35 & 3.97 & 2.75 & 2.75 \\ 3.19 & 2.88 & 2.75 & 3.97 & 2.75 \\ 3.19 & 2.88 & 2.75 & 2.75 & 3.97 \end{pmatrix},$$

$$U_{mm'}^{\sigma\sigma} = \begin{pmatrix} 0 & 2.10 & 2.01 & 2.70 & 2.70 \\ 2.10 & 0 & 2.94 & 2.24 & 2.24 \\ 2.01 & 2.94 & 0 & 2.15 & 2.15 \\ 2.70 & 2.24 & 2.15 & 0 & 2.15 \\ 2.70 & 2.24 & 2.15 & 2.15 & 0 \end{pmatrix}.$$

SrCrO_3

$$U_{mm'}^{\sigma\bar{\sigma}} = \begin{pmatrix} 3.84 & 2.39 & 2.40 & 2.87 & 2.87 \\ 2.39 & 3.84 & 3.02 & 2.56 & 2.56 \\ 2.40 & 3.02 & 3.89 & 2.59 & 2.59 \\ 2.87 & 2.56 & 2.59 & 3.89 & 2.59 \\ 2.87 & 2.56 & 2.59 & 2.59 & 3.89 \end{pmatrix},$$

$$U_{mm'}^{\sigma\sigma} = \begin{pmatrix} 0 & 1.66 & 1.67 & 2.38 & 2.38 \\ 1.66 & 0 & 2.61 & 1.91 & 1.91 \\ 1.67 & 2.61 & 0 & 1.94 & 1.94 \\ 2.38 & 1.91 & 1.94 & 0 & 1.94 \\ 2.38 & 1.91 & 1.94 & 1.94 & 0 \end{pmatrix}.$$

SrMnO_3

$$U_{mm'}^{\sigma\bar{\sigma}} = \begin{pmatrix} 3.62 & 2.17 & 2.25 & 2.74 & 2.74 \\ 2.17 & 3.62 & 2.90 & 2.41 & 2.41 \\ 2.25 & 2.90 & 3.90 & 2.52 & 2.51 \\ 2.74 & 2.41 & 2.52 & 3.91 & 2.52 \\ 2.74 & 2.41 & 2.51 & 2.52 & 3.90 \end{pmatrix},$$

$$U_{mm'}^{\sigma\sigma} = \begin{pmatrix} 0 & 1.44 & 1.49 & 2.22 & 2.22 \\ 1.44 & 0 & 2.47 & 1.73 & 1.73 \\ 1.49 & 2.47 & 0 & 1.81 & 1.81 \\ 2.22 & 1.73 & 1.81 & 0 & 1.81 \\ 2.22 & 1.73 & 1.81 & 1.81 & 0 \end{pmatrix}.$$

APPENDIX D : Reduced interaction matrices for Sr_2MO_4 ($M = \text{Mo, Tc, Ru, Rh}$)

“ d - dp Hamiltonian”

The reduced interaction matrices within the d - dp model (Tab. V) and calculated with cubic symmetry, are given below for the layered perovskites. The ordering of the orbitals in these matrices is $d_{z^2}, d_{x^2-y^2}, d_{xy}, d_{xz}, d_{yz}$. The values are given in eV.

Sr_2MoO_4

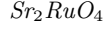
$$U_{mm'}^{\sigma\bar{\sigma}} = \begin{pmatrix} 4.20 & 3.04 & 2.90 & 3.22 & 3.22 \\ 3.04 & 4.35 & 3.43 & 3.06 & 3.05 \\ 2.90 & 3.43 & 3.97 & 2.93 & 2.92 \\ 3.22 & 3.06 & 2.93 & 3.86 & 2.89 \\ 3.22 & 3.05 & 2.92 & 2.89 & 3.84 \end{pmatrix},$$

$$U_{mm'}^{\sigma\sigma} = \begin{pmatrix} 0 & 2.48 & 2.38 & 2.83 & 2.83 \\ 2.48 & 0 & 3.10 & 2.56 & 2.55 \\ 2.38 & 3.10 & 0 & 2.44 & 2.44 \\ 2.83 & 2.56 & 2.44 & 0 & 2.41 \\ 2.83 & 2.55 & 2.44 & 2.41 & 0 \end{pmatrix}.$$

Sr_2TcO_4

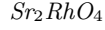
$$U_{mm'}^{\sigma\bar{\sigma}} = \begin{pmatrix} 4.06 & 2.88 & 2.81 & 3.13 & 3.13 \\ 2.88 & 4.23 & 3.38 & 2.96 & 2.96 \\ 2.81 & 3.38 & 4.04 & 2.90 & 2.90 \\ 3.13 & 2.96 & 2.90 & 3.86 & 2.84 \\ 3.13 & 2.96 & 2.90 & 2.84 & 3.86 \end{pmatrix},$$

$$U_{mm'}^{\sigma\sigma} = \begin{pmatrix} 0 & 2.29 & 2.25 & 2.72 & 2.72 \\ 2.29 & 0 & 3.04 & 2.44 & 2.44 \\ 2.25 & 3.04 & 0 & 2.38 & 2.38 \\ 2.72 & 2.44 & 2.38 & 0 & 2.33 \\ 2.72 & 2.44 & 2.38 & 2.33 & 0 \end{pmatrix}.$$



$$U_{mm'}^{\sigma\bar{\sigma}} = \begin{pmatrix} 4.06 & 2.83 & 2.78 & 3.17 & 3.18 \\ 2.83 & 4.22 & 3.37 & 2.98 & 2.99 \\ 2.78 & 3.37 & 4.07 & 2.94 & 2.95 \\ 3.17 & 2.98 & 2.94 & 4.02 & 2.93 \\ 3.18 & 2.99 & 2.95 & 2.93 & 4.05 \end{pmatrix},$$

$$U_{mm'}^{\sigma\sigma} = \begin{pmatrix} 0 & 2.22 & 2.19 & 2.73 & 2.74 \\ 2.22 & 0 & 3.01 & 2.42 & 2.44 \\ 2.19 & 3.01 & 0 & 2.39 & 2.39 \\ 2.73 & 2.42 & 2.39 & 0 & 2.38 \\ 2.74 & 2.44 & 2.39 & 2.38 & 0 \end{pmatrix}.$$



$$U_{mm'}^{\sigma\bar{\sigma}} = \begin{pmatrix} 4.18 & 2.93 & 2.95 & 3.37 & 3.38 \\ 2.93 & 4.34 & 3.55 & 3.15 & 3.16 \\ 2.95 & 3.55 & 4.37 & 3.18 & 3.19 \\ 3.37 & 3.15 & 3.18 & 4.39 & 3.20 \\ 3.38 & 3.16 & 3.19 & 3.20 & 4.44 \end{pmatrix},$$

$$U_{mm'}^{\sigma\sigma} = \begin{pmatrix} 0 & 2.29 & 2.31 & 2.92 & 2.94 \\ 2.29 & 0 & 3.17 & 2.56 & 2.58 \\ 2.31 & 3.17 & 0 & 2.57 & 2.58 \\ 2.92 & 2.56 & 2.57 & 0 & 2.59 \\ 2.94 & 2.58 & 2.58 & 2.59 & 0 \end{pmatrix}.$$

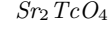
“ t_{2g} - t_{2g} Hamiltonian”

We give below the reduced interaction matrices for the t_{2g} local orbitals within the t_{2g} - t_{2g} model. The Hubbard-Kanamori parameters, \mathcal{U} and \mathcal{U}' , shown in Table VII correspond to the orbital average, $U_{mm}^{\sigma\bar{\sigma}}, U_{m \neq m'}^{\sigma\bar{\sigma}}$ (Eqs. 19 and 21), respectively. The exchange parameter, \mathcal{J} , corresponds to the orbital average of $J_{mm'} = (U_{mm'}^{\sigma\bar{\sigma}} - U_{mm'}^{\sigma\sigma})(1 - \delta_{mm'})$ (Eq. 20). The ordering of the orbitals is (d_{xy}, d_{xz}, d_{yz}) .



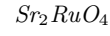
$$U_{mm'}^{\sigma\bar{\sigma}} = \begin{pmatrix} 2.96 & 2.19 & 2.19 \\ 2.19 & 2.68 & 2.09 \\ 2.19 & 2.09 & 2.68 \end{pmatrix},$$

$$U_{mm'}^{\sigma\sigma} = \begin{pmatrix} 0.00 & 1.89 & 1.89 \\ 1.89 & 0.00 & 1.82 \\ 1.89 & 1.82 & 0.00 \end{pmatrix}.$$



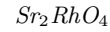
$$U_{mm'}^{\sigma\bar{\sigma}} = \begin{pmatrix} 2.89 & 2.10 & 2.10 \\ 2.10 & 2.61 & 2.01 \\ 2.10 & 2.01 & 2.61 \end{pmatrix},$$

$$U_{mm'}^{\sigma\sigma} = \begin{pmatrix} 0.00 & 1.81 & 1.81 \\ 1.81 & 0.00 & 1.74 \\ 1.81 & 1.74 & 0.00 \end{pmatrix}.$$



$$U_{mm'}^{\sigma\bar{\sigma}} = \begin{pmatrix} 2.72 & 1.97 & 1.97 \\ 1.97 & 2.48 & 1.89 \\ 1.97 & 1.89 & 2.48 \end{pmatrix},$$

$$U_{mm'}^{\sigma\sigma} = \begin{pmatrix} 0.00 & 1.71 & 1.71 \\ 1.71 & 0.00 & 1.65 \\ 1.71 & 1.65 & 0.00 \end{pmatrix}.$$



$$U_{mm'}^{\sigma\bar{\sigma}} = \begin{pmatrix} 1.81 & 1.16 & 1.20 \\ 1.16 & 1.69 & 1.19 \\ 1.20 & 1.19 & 1.77 \end{pmatrix},$$

$$U_{mm'}^{\sigma\sigma} = \begin{pmatrix} 0.00 & 0.93 & 0.96 \\ 0.93 & 0.00 & 0.97 \\ 0.96 & 0.97 & 0.00 \end{pmatrix}.$$

-
- * Loig.Vaugier@cphpt.polytechnique.fr
† h.jiang@pku.edu.cn
‡ Silke.Biermann@cphpt.polytechnique.fr
- ¹ M. Imada, A. Fujimori, and Y. Tokura, *Rev. Mod. Phys.* **70**, 1039 (1998).
 - ² W. Kohn, *Rev. Mod. Phys.* **71**, 1253 (1999).
 - ³ P. Hohenberg and W. Kohn, *Phys. Rev.* **136**, B864 (1964).
 - ⁴ W. Kohn and L. J. Sham, *Phys. Rev.* **140**, A1133 (1965).
 - ⁵ R. O. Jones and O. Gunnarsson, *Rev. Mod. Phys.* **61**, 689 (1989).
 - ⁶ V. I. Anisimov, F. Aryasetiawan, and A. I. Lichtenstein, *J. Phys. Condens. Matter* **9**, 767 (1997).
 - ⁷ V. I. Anisimov, A. Poteryaev, M. Korotin, A. Anokhin, and G. Kotliar, *J. Phys. Condens. Matter* **9**, 943 (1997).
 - ⁸ A. I. Lichtenstein and M. I. Katsnelson, *Phys. Rev. B* **57**, 6884 (1998).
 - ⁹ G. Kotliar, S. Y. Savrasov, K. Haule, V. S. Oudovenko, O. Parcollet, and C. A. Marianetti, *Rev. Mod. Phys.* **78**, 865 (2006).
 - ¹⁰ F. Aryasetiawan, M. Imada, A. Georges, G. Kotliar, S. Biermann, and A. I. Lichtenstein, *Phys. Rev. B* **70**, 195104 (2004).
 - ¹¹ P. Löwdin, *J. Chem. Phys.* **19**, 1396 (1951).
 - ¹² O. K. Andersen and T. Saha-Dasgupta, *Phys. Rev. B* **62**, R16219 (2000).
 - ¹³ P. Blaha, K. Schwarz, G. Madsen, D. Kvasnicka, and J. Luitz, *Wien2k, An Augmented Plane Wave+Local Orbitals Program for Calculating Crystal Properties* (Tech. Universität Wien, Austria, 2001).
 - ¹⁴ M. Aichhorn, L. Pourovskii, V. Vildosola, M. Ferrero, O. Parcollet, T. Miyake, A. Georges, and S. Biermann, *Phys. Rev. B* **80**, 085101 (2009).
 - ¹⁵ E. Antonides, E. C. Janse, and G. A. Sawatzky, *Phys. Rev. B* **15**, 1669 (1977).
 - ¹⁶ G. A. Sawatzky and J. W. Allen, *Phys. Rev. Lett.* **53**, 2339 (1984).
 - ¹⁷ J. Hubbard, *Proc. R. Soc. London A* **276**, 238 (1963).
 - ¹⁸ J. Kanamori, *Prog. Theor. Phys.* **30**, 275 (1963).
 - ¹⁹ M. C. Gutzwiller, *Phys. Rev. Lett.* **10**, 159 (1963).
 - ²⁰ D. K. G. de Boer, C. Haas, and G. A. Sawatzky, *J. Phys. F* **14**, 2769 (1984).
 - ²¹ J. Ghijsen, L. H. Tjeng, H. Eskes, G. A. Sawatzky, and R. L. Johnson, *Phys. Rev. B* **42**, 2268 (1990).
 - ²² D. van der Marel, Ph.D. thesis, Rijksuniversiteit Groningen (1985).
 - ²³ B. R. Judd, *Operator Techniques in Atomic Spectroscopy* (Princeton University Press, 1998).
 - ²⁴ S. Sugano, Y. Tanabe, and H. Kamimura, *Multiplets of transition-metal ions in crystal*, vol. 1 (Academic Press, New York London, 1970).
 - ²⁵ P. H. Dederichs, S. Blügel, R. Zeller, and H. Akai, *Phys. Rev. Lett.* **53**, 2512 (1984).
 - ²⁶ A. K. McMahan, R. M. Martin, and S. Satpathy, *Phys. Rev. B* **38**, 6650 (1988).
 - ²⁷ M. S. Hybertsen, M. Schlüter, and N. E. Christensen, *Phys. Rev. B* **39**, 9028 (1989).
 - ²⁸ O. Gunnarsson, O. K. Andersen, O. Jepsen, and J. Zaanen, *Phys. Rev. B* **39**, 1708 (1989).
 - ²⁹ O. Gunnarsson, *Phys. Rev. B* **41**, 514 (1990).
 - ³⁰ V. I. Anisimov and O. Gunnarsson, *Phys. Rev. B* **43**, 7570 (1991).
 - ³¹ G. K. H. Madsen and P. Novák, *Eur. Phys. Lett.* **69**, 777 (2005).
 - ³² K. Nakamura, R. Arita, Y. Yoshimoto, and S. Tsuneyuki, *Phys. Rev. B* **74**, 235113 (2006).
 - ³³ W. E. Pickett, S. C. Erwin, and E. C. Ethridge, *Phys. Rev. B* **58**, 1201 (1998).
 - ³⁴ M. Cococcioni and S. de Gironcoli, *Phys. Rev. B* **71**, 035105 (2005).
 - ³⁵ I. V. Solov'yev and M. Imada, *Phys. Rev. B* **71**, 045103 (2005).
 - ³⁶ T. Miyake and F. Aryasetiawan, *Phys. Rev. B* **77**, 085122 (2008).
 - ³⁷ E. Şaşioğlu, C. Friedrich, and S. Blügel, *Phys. Rev. B* **83**, 121101 (2011).
 - ³⁸ T. Miyake, K. Nakamura, R. Arita, and M. Imada, *J. Phys. Soc. Jpn.* **79**, 044705 (2010).
 - ³⁹ F. Aryasetiawan, K. Karlsson, O. Jepsen, and U. Schönberger, *Phys. Rev. B* **74**, 125106 (2006).
 - ⁴⁰ T. Miyake, F. Aryasetiawan, and M. Imada, *Phys. Rev. B* **80**, 155134 (2009).
 - ⁴¹ J. M. Tomczak, T. Miyake, R. Sakuma, and F. Aryasetiawan, *Phys. Rev. B* **79**, 235133 (2009).
 - ⁴² K. Karlsson, F. Aryasetiawan, and O. Jepsen, *Phys. Rev. B* **81**, 245113 (2010).
 - ⁴³ M. Aichhorn, S. Biermann, T. Miyake, A. Georges, and M. Imada, *Phys. Rev. B* **82**, 064504 (2010).
 - ⁴⁴ J. Mravlje, M. Aichhorn, T. Miyake, K. Haule, G. Kotliar, and A. Georges, *Phys. Rev. Lett.* **106**, 096401 (2011).
 - ⁴⁵ C. Martins, M. Aichhorn, L. Vaugier, and S. Biermann, *Phys. Rev. Lett.* **107**, 266404 (2011).
 - ⁴⁶ S. Biermann, F. Aryasetiawan, and A. Georges, *Phys. Rev. Lett.* **90**, 086402 (2003).
 - ⁴⁷ P. Sun and G. Kotliar, *Phys. Rev. B* **66**, 085120 (2002).
 - ⁴⁸ F. Aryasetiawan, J. M. Tomczak, T. Miyake, and R. Sakuma, *Phys. Rev. Lett.* **102**, 176402 (2009).
 - ⁴⁹ A. Kutepov, K. Haule, S. Y. Savrasov, and G. Kotliar, *Phys. Rev. B* **82**, 045105 (2010).
 - ⁵⁰ M. Imada and T. Miyake, *J. Phys. Soc. Jpn.* **79**, 112001 (2010).
 - ⁵¹ L. Vaugier, Ph.D. thesis, Ecole Polytechnique, France (2011).
 - ⁵² Y. Nomura, M. Kaltak, K. Nakamura, C. Taranto, S. Sakai, A. Toschi, R. Arita, K. Held, G. Kresse, and M. Imada, *arXiv* **1205.2836** (2012).
 - ⁵³ M. Casula, A. Rubtsov, and S. Biermann, *Phys. Rev. B* **85**, 035115 (2012).
 - ⁵⁴ P. Werner, M. Casula, T. Miyake, F. Aryasetiawan, A. J. Millis, and S. Biermann, *Nature Physics* **8**, 331 (2012).
 - ⁵⁵ M. Casula, P. Werner, L. Vaugier, F. Aryasetiawan, A. J. Millis, and S. Biermann, *arXiv* **1204.4900** (2012).
 - ⁵⁶ T. Miyake, L. Pourovskii, V. Vildosola, S. Biermann, and A. Georges, *J. Phys. Soc. Jpn. : Supplement C* **77**, 99 (2008).
 - ⁵⁷ J. C. Slater, *Quantum Theory of Atomic Structure*, vol. 1 (McGraw-Hill, New York, 1960).
 - ⁵⁸ V. I. Anisimov, I. V. Solov'yev, M. A. Korotin, M. T. Czyżyk, and G. A. Sawatzky, *Phys. Rev. B* **48**, 16929 (1993).
 - ⁵⁹ Y. S. Lee, J. S. Lee, T. W. Noh, D. Y. Byun, K. S. Yoo, K. Yamaura, and E. Takayama-Muromachi, *Phys. Rev. B* **67**, 113101 (2003).

- ⁶⁰ J. Torrance, L. P., A. C., and R. Metzger, *Physica C* **182**, 351 (1991).
- ⁶¹ A. Georges, Lectures on the physics of highly correlated electron systems VI **715**, 3 (2004).
- ⁶² J. Zaanen, G. A. Sawatzky, and J. W. Allen, *Phys. Rev. Lett.* **55**, 418 (1985).
- ⁶³ A. Sekiyama, H. Fujiwara, S. Imada, S. Suga, H. Eisaki, S. I. Uchida, K. Takegahara, H. Harima, Y. Saitoh, I. A. Nekrasov, et al., *Phys. Rev. Lett.* **93**, 156402 (2004).
- ⁶⁴ R. Eguchi, T. Kiss, S. Tsuda, T. Shimojima, T. Mizokami, T. Yokoya, A. Chainani, S. Shin, I. H. Inoue, T. Togashi, et al., *Phys. Rev. Lett.* **96**, 076402 (2006).
- ⁶⁵ A. Fujimori, I. Hase, H. Namatame, Y. Fujishima, Y. Tokura, H. Eisaki, S. Uchida, K. Takegahara, and F. M. F. de Groot, *Phys. Rev. Lett.* **69**, 1796 (1992).
- ⁶⁶ T. Yoshida, K. Tanaka, H. Yagi, A. Ino, H. Eisaki, A. Fujimori, and Z.-X. Shen, *Phys. Rev. Lett.* **95**, 146404 (2005).
- ⁶⁷ K. Morikawa, T. Mizokawa, K. Kobayashi, A. Fujimori, H. Eisaki, S. Uchida, F. Iga, and Y. Nishihara, *Phys. Rev. B* **52**, 13711 (1995).
- ⁶⁸ F. Lechermann, A. Georges, A. Poteryaev, S. Biermann, M. Posternak, A. Yamasaki, and O. K. Andersen, *Phys. Rev. B* **74**, 125120 (2006).
- ⁶⁹ B. Chamberland, *Solid State Commun.* **5**, 663 (1967).
- ⁷⁰ J.-S. Zhou, C.-Q. Jin, Y.-W. Long, L.-X. Yang, and J. B. Goodenough, *Phys. Rev. Lett.* **96**, 046408 (2006).
- ⁷¹ L. Ortega-San-Martin, A. J. Williams, J. Rodgers, J. P. Attfield, G. Heymann, and H. Huppertz, *Phys. Rev. Lett.* **99**, 255701 (2007).
- ⁷² K.-W. Lee and W. E. Pickett, *Phys. Rev. B* **80**, 125133 (2009).
- ⁷³ Y. Qian, G. Wang, Z. Li, C. Jin, and Z. Fang, *New Journal of Physics* **13**, 053002 (2011).
- ⁷⁴ A. Daoud-Aladine, C. Martin, L. C. Chapon, M. Hervieu, K. S. Knight, M. Brunelli, and P. G. Radaelli, *Phys. Rev. B* **75**, 104417 (2007).
- ⁷⁵ T. Takeda and S. Ohara, *J. Phys. Soc. Jpn.* **37**, 275 (1974).
- ⁷⁶ R. Søndena, P. Ravindran, S. Stølen, T. Grande, and M. Hanfland, *Phys. Rev. B* **74**, 144102 (2006).
- ⁷⁷ O. Chmaissem, B. Dabrowski, S. Kolesnik, J. Mais, D. E. Brown, R. Kruk, P. Prior, B. Pyles, and J. D. Jorgensen, *Phys. Rev. B* **64**, 134412 (2001).
- ⁷⁸ T. Saitoh, A. E. Bocquet, T. Mizokawa, and A. Fujimori, *Phys. Rev. B* **52**, 7934 (1995).
- ⁷⁹ A. E. Bocquet, T. Mizokawa, K. Morikawa, A. Fujimori, S. R. Barman, K. Maiti, D. D. Sarma, Y. Tokura, and M. Onoda, *Phys. Rev. B* **53**, 1161 (1996).
- ⁸⁰ J.-S. Kang, H. J. Lee, G. Kim, D. H. Kim, B. Dabrowski, S. Kolesnik, H. Lee, J.-Y. Kim, and B. I. Min, *Phys. Rev. B* **78**, 054434 (2008).
- ⁸¹ D. van der Marel, G. A. Sawatzky, and F. U. Hillebrecht, *Phys. Rev. Lett.* **53**, 206 (1984).
- ⁸² H. Hannerz, G. Svensson, S. Y. Istomin, and O. G. D'yachenko, *Journal of Solid State Chemistry* **147**, 421 (1999).
- ⁸³ K. Isawa, J. Sugiyama, K. Matsuura, A. Nozaki, and H. Yamauchi, *Phys. Rev. B* **47**, 2849 (1993).
- ⁸⁴ I. Nagai, N. Shirakawa, S. Ikeda, I. R., H. Nishimura, and M. Kosaka, *Appl. Phys. Lett.* **87**, 024105 (2005).
- ⁸⁵ E. E. Rodriguez, F. Poineau, A. Llobet, B. J. Kennedy, M. Avdeev, G. J. Thorogood, M. L. Carter, R. Seshadri, D. J. Singh, and A. K. Cheetham, *Phys. Rev. Lett.* **106**, 067201 (2011).
- ⁸⁶ C. Franchini, T. Archer, J. He, X.-Q. Chen, A. Filippetti, and S. Sanvito, *Phys. Rev. B* **83**, 220402 (2011).
- ⁸⁷ S. Middey, A. Kumar Nandy, P. Mahadevan, and D. D. Sarma, *arXiv* **1112.5587v1** (2011).
- ⁸⁸ J. Mravlje, M. Aichhorn, and A. Georges, *Phys. Rev. Lett.* **108**, 197202 (2012).
- ⁸⁹ S.-I. Ikeda, N. Shirakawa, H. Bando, and Y. Ootuka, *J. Phys. Soc. Jpn.* **69**, 3162 (2000).
- ⁹⁰ N. E. Hussey, A. P. Mackenzie, J. R. Cooper, Y. Maeno, S. Nishizaki, and T. Fujita, *Phys. Rev. B* **57**, 5505 (1998).
- ⁹¹ A. P. Mackenzie and Y. Maeno, *Rev. Mod. Phys.* **75**, 657 (2003).
- ⁹² A. Liebsch and A. Lichtenstein, *Phys. Rev. Lett.* **84**, 1591 (2000).
- ⁹³ V. I. Anisimov, I. A. Nekrasov, D. E. Kondakov, T. M. Rice, and M. Sigrist, *Eur. Phys. Lett.* **25**, 191 (2002).
- ⁹⁴ Z. V. Pchelkina, I. A. Nekrasov, T. Pruschke, A. Sekiyama, S. Suga, V. I. Anisimov, and D. Vollhardt, *Phys. Rev. B* **75**, 035122 (2007).
- ⁹⁵ Q. Huang, J. L. Soubeyroux, O. Chmaissem, I. Natali Sora, A. Santoro, R. J. Cava, J. J. Krajewski, and W. F. Peck, *Journal of Solid State Chemistry* **112**, 355 (1994).
- ⁹⁶ S. J. Moon, M. W. Kim, K. W. Kim, Y. S. Lee, J.-Y. Kim, J.-H. Park, B. J. Kim, S.-J. Oh, S. Nakatsuji, Y. Maeno, et al., *Phys. Rev. B* **74**, 113104 (2006).
- ⁹⁷ A. Tamai, M. P. Allan, J. F. Mercure, W. Meevasana, R. Dunkel, D. H. Lu, R. S. Perry, A. P. Mackenzie, D. J. Singh, Z.-X. Shen, et al., *Phys. Rev. Lett.* **101**, 026407 (2008).
- ⁹⁸ M. W. Haverkort, I. S. Elfimov, L. H. Tjeng, G. A. Sawatzky, and A. Damascelli, *Phys. Rev. Lett.* **101**, 026406 (2008).
- ⁹⁹ G.-Q. Liu, V. N. Antonov, O. Jepsen, and O. K. Andersen, *Phys. Rev. Lett.* **101**, 026408 (2008).
- ¹⁰⁰ M. W. Haverkort, Ph.D. thesis, Universität Köln (2005).
- ¹⁰¹ B.-C. Shih, Y. Zhang, W. Zhang, and P. Zhang, *Phys. Rev. B* **85**, 045132 (2012).
- ¹⁰² H. Jiang, R. Gómez-Abal, X. Li, C. Meisenbichler, C. Ambrosch-Draxl, and M. Scheffler, (unpublished) (2012).
- ¹⁰³ F. Aryasetiawan and O. Gunnarsson, *Rep. Prog. Phys.* **61**, 237 (1998).
- ¹⁰⁴ T. Kotani and M. van Schilfgaarde, *Solid State Commun.* **121**, 461 (2002).